ABSTRACT

Title of Thesis:	HIGH ENERGY ZINC BATTERY SYSTEM WITH AN EXTREMELY WIDE OPERATING TEMPERATURE WINDOW
	Tingting Qing, Master of Science, 2018
Thesis directed by:	Professor Chunsheng Wang, Department of Chemical and Biomolecular Engineering

Military and planetary application requires high energy density rechargeable battery with an extremely wide operating temperature range. Current rechargeable batteries only operate in a narrow range from -20 ℃ to 60 ℃. Low ionic conductivity of electrolyte and sluggish lithium ion diffusion of electrode at a low temperature, the irreversible phase transition at elevated temperature limit broadening operating temperature range of battery. In this research, a novel zinc battery $LiFePO_4/Li_2ZnCl_4.9H_2O/Zn$ with wide operating temperature range between -70 ℃ and 70 ℃ has been developed. The $Li_2ZnCl_4.9H_2O$ electrolyte has very high ionic conductivity at -70 ℃, while the PEDOT coating on $LiFePO_4$ reduce the side reaction at 70 ℃. At 70 ℃, $LiFePO_4$@PEDOT/Li_2ZnCl_4.9H2O/Zn cells provide a capacity of 130 $mAh.g^{-1}$ achieved over 20 cycles at 0.3 C, with a high rate capability. It also showed a stable cycling at -70 ℃ with 133 $mAh.g^{-1}$ for 50 cycles at 0.1 C.

HIGH ENERGY ZINC BATTERY SYSTEM WITH AN EXTREME WIDE OPERATING TEMPERATURE WINDOW

by

Tingting Qing

Thesis submitted to the Faculty of the Graduate School of the
University of Maryland, College Park, in partial fulfillment
of the requirements for the degree of
Master of Science
2018

Advisory Committee:
Professor Chunsheng Wang, Chair
Professor Dongxia Liu
Professor Taylor J. Woehl

Acknowledgements

I would first like to express my sincere gratitude to my advisor Prof. Chunsheng Wang for his guidance and support throughout my whole research and thesis.

I would like to thank my colleagues, Dr. Chongyin Yang, Mr. Nico Edison, Dr. Ji chen and Dr. Yujia Liang as well. We spent lots of energy and time on discussing my works to optimize my experiment. Mr. Nico Edison and his colleagues in the Army Rsearch Lab helped me with all the tests at low temperature, including the electrochemical testing, DSC testing. Mr. Ji Chen helped me characterization with XRD and Raman test. Dr. Yujiang Liang helped me with TEM test. Without their passionate and careful favor, my experiment could not have been processed successfully.

I also would like to thank my group members, Dr. Xiulin Fan, Dr. Fei Wang, Dr. Chao Luo, Dr. Long Chen, Dr. Ji Chen, Dr. Fudong Han, Ms. Singyuk Hou, Ms. Ji Zheng, Mr. Xiao Ji, Mr. Minglei Mao, Mr. Chunyu Cui for their great help to my research.

Finally and most importantly, I would like to thank my parents sincerely. Without their constant support and care, I could not have the opportunity to complete my graduate study. I feel grateful to have such a lovely hom

Table of Contents

Acknowledgements ii
List of Tables iv
Chapter 1: Introduction 1
1.1 Demand for Renewable Energy Source 1
1.2 Aqueous Rechargeable Lithium-ion Battery (ARLB) 4
1.2.1 Aqueous electrolytes 4
1.2.2 Electrochemical stability window of aqueous electrolytes 5
1.2.3 Advantages and disadvantages of aqueous electrolytes 6
1.3 Superionic electrolytes 8
1.4 Rechargeable Zinc Battery 9
1.4.1 Advantages of zinc battery 9
1.4.2 Challenges for development of zinc battery 10
1.4.3 Hybrid battery of LiFePO4/Zn 12
1.5 Cathode Material: $LiFePO_4$ at extreme temperature 14
1.5.1 Effects of high temperature on batteries 14
1.5.2 Effects of low temperature on batteries 15
1.5.3 LiFePO4 at high temperature 16
1.5.4 LiFePO4 at low temperature 17
1.6 Poly (3, 4-rthylenediocythiophene) 18
1.6.1 Application of PEDOT in batteries 18
1.6.2 The Synthesis of PEDOT 20
Chapter 2: Theory and Experiment 21
2.1Material Synthesis and Preparation of Electrolytes 21
2.1.1 Different amounts of PEDOT coating on LiFePO4 21
2.1.2 Electrolytes of Li2ZnCl4.xH2O 22
2.2 Characterization Methods 22
2.2.1 Electrolytes and powder characterization 22
2.3 Electrochemical Measurement Technology 23
2.3.1 Cyclic Voltammetry 23
2.3.2 Electrochemical performance 25
Chapter 3: Characterization Discussion and Results 28
3.1 Raman and XRD Characterization 28
3.2 Measurement of Ionic Conductivity of $Li_2ZnCl_4.9H_2O$ 32
3.3 Analysis of Thermal Stability on $Li_2ZnCl_4.xH_2O$ 33
3.4 TEM Characterization of PEDOT-coated $LiFePO_4$ 36
3.5 Cyclic Voltammetry for Electrochemical Stability Window 37
Chapter 4: Electrochemical Performance at extreme temperatures 39
4.1 Electrochemical Performance at room temperature 39
4.2 Electrochemical Performance at 70 ℃ 41
4.3 Electrochemical Performance at -70 ℃ 46
Chapter 5: Conclusion 49
Chapter 6: Future Work 50

List of Tables

Table 1.1 Various types of major secondary batteries on a cell level……3

Table 2.1 Three Ratio of $LeFePO_4$ and EDOT in the synthesis……20

Table 3.1 Structure parameters of Li_2ZnCl_4…… 26

List of Figures

Figure 1.1 Illustration of the six forms of energy and related examples of their interconversion ……2

Figure 1.2 Illustration of the charge/discharge process involved in a lithium ion cell consisting of graphite as the anode and layered $LiCoO_2$ as the cathode……3

Figure 1.3 Spinel structure of Li_2ZnCl_4, the interstitial sites and ionic conduction pathway are indicated…… 9

Figure 1.4 Cathode and anode candidates for the hybrid battery ……13

Figure 1.5 Summary of energy densities and temperature windows of commercially rechargeable batteries……16

Figure 1.6 Structure of PEDOT…… 18

Figure 2.1 (a) the excitation signal of CV. (b) CV curve with the potential versus reference electrode……24

Figure 2.2 Schematic graph of the cell assembled for electrochemical test……25

Figure 3.1 XRD pattern of the dehydrated Li_2ZnCl_4 sample……27

Figure 3.2 Raman spectra of seven different concentrations of $Li_2ZnCl_4.xH_2O$ (x=6, 9, 12, 22.5, 72, 156) ……29

Figure 3.3 Raman spectra of solid $ZnCl_2$ and LiCl powders……30

Figure 3.4 Raman spectra of five solutions of (2+y) $Li_2ZnCl_4.9H_2O$ (y=0.4, 0.2, 0, -0.2, -0.4) ……31

Figure 3.5 the ionic conductivity of $Li_2ZnCl_4.9H_2O$ measured from 80 ℃ to -75 ℃……32

Figure 3.6 DSC-TGA curves if pure water and $Li_2ZnCl_4.xH_2O$ (x=6, 9, 12), heating in argon flow of 100 $ml.min^{-1}$ at a rate of 5 ℃.min^{-1} from 25 ℃ and 350 ℃, weight-loss curves (green) and heat flow curves (blue) ……34

Figure 3.7 DSC curves of $Li_2ZnCl_4.xH_2O$ (x=6, 9, 12), cooling rate of 5 ℃.min^{-1} from room temperature to -145 ℃……35

Figure 3.8 TEM image of the tested c-LFP2 sample……36

Figure 3.9 CV measurement of expandable graphite/ $Li_2ZnCl_4.9H_2O$/ activated carbon cell in the voltage range between 2.2 V and 4.5 V versus Li/Li^+ at the scanning rate of 5$mV.s^{-1}$……37

Figure 4.1 Cycling performance of PEDOT-coated $LiFePO_4$ electrodes, c-LFP1 (blue), c-LFP2 (red), c-LFP3 (green), comparing with uncoated $LiFePO_4$, u-LFP (black) (current density= 0.3 C, temperature=25 ℃) ……39

Figure 4.2 Charge-discharge curves of PEDOT-coated $LiFePO_4$ electrodes, c-LFP1 (blue), c-LFP2 (red), c-LFP3 (green), comparing with uncoated $LiFePO_4$, u-LFP (black) (current density= 0.3 C, temperature=25 ℃) ……40

Figure 4.3 Cycling performance of $Li_2ZnCl_4.6H_2O$ (blue), $Li_2ZnCl_4.9H_2O$ (black), $Li_2ZnCl_4.12H_2O$ (red) with different electrodes c-LFP1(a), c-LFP2 (b), c-LFP3 (c), respectively during 20 cycles (current density= 0.3 C, temperature=70 ℃)……42

Figure 4.4 Charge curves of c-LFP2 (solid line) electrode comparing with u-LFP (dash line) electrode in $Li_2ZnCl_4.9H_2O$ (current density= 0.3 C, temperature=70 ℃) ……44

Figure 4.5 Rate capability of c-LFP2 electrode in $Li_2ZnCl_4.9H_2O$ at different current densities during 30 cycles (temperature=70 ℃) ……45

Figure 4.6 Discharge curves of c-LFP2 electrode in $Li_2ZnCl_4.9H_2O$ (current density= 0.1 C, temperature=-70 ℃) ……46

Figure 4.7 Cycling performance of c-LFP2 electrode in $Li_2ZnCl_4.9H_2O$ during 50 cycles (current density= 0.1 C, temperature=-70 ℃) ……47

Chapter 1: Introduction

1.1 Demand for Renewable Energy Source

Nowadays, energy industry mainly depends on the increasing demand of various non-renewable energy such as coal, gasoline and natural gas. However, the massive consumption of fossil fuel contributes to economic and environmental problems. For the environment and conventional energy replacement's sake, it is crucial to seek a new kind of renewable and environmentally-friendly energy source as the candidate of fossil fuel. Various renewable energy, electrical energy, solar energy and nuclear energy etc., are introduced to the public. Fig 1.1 shows the interconversion of six main forms of energy. Electrical energy is the most convenient source due to its broad distribution, easy conversion processes and no dangerous leaks[1]. Thus, numerous applications of secondary galvanic cells play a crucial role in the future, such as battery packs for electrical vehicles (EVs), small capacity units for microelectronics. However, rechargeable batteries' advances are quietly slow due to the complex interaction with heterogeneous system[1].

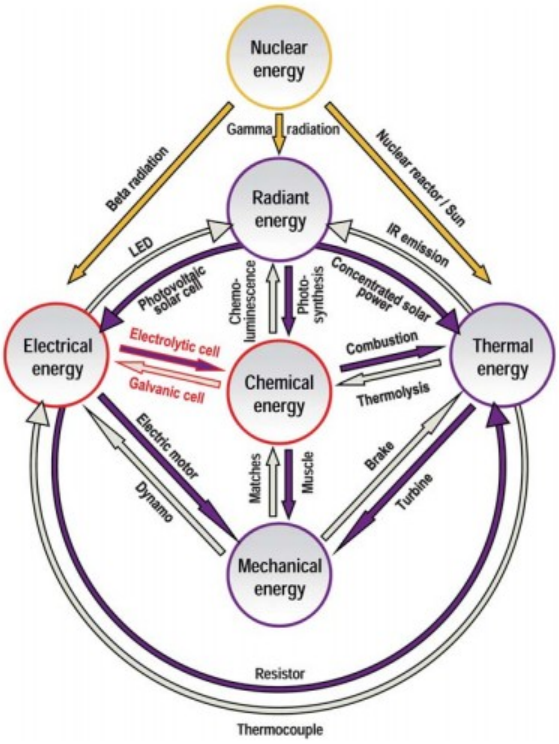

Figure 1.1 the six forms of energy and related examples of their mutual conversion[1]

Rechargeable batteries spontaneously convert chemical energy to electrical energy through a reversible application of oxidation-reduction reaction. During discharging, two separate electrochemical reactions, the release of electronics by reduction at the anode and the take-up of electronic by oxidation at the cathodes, can occur by the external electric circuit and ionic current in the electrolytes, as shown in Fig 1.2. During charging, electrochemical reactions can happen in the reverse directions proves by achieving an external electromotive force. It is processed when taking electrons from the positive electrode and putting electrons back to negative anode. An electrochemical cell can be evaluated by some electrical criteria such as

the faradic stored capacity denoted Q normalized per unit of mass ($Ah.kg^{-1}$) or volume ($Ah.L^{-1}$) and the energy density ($Wh.kg^{-1}$ or $Wh.L^{-1}$) [1].

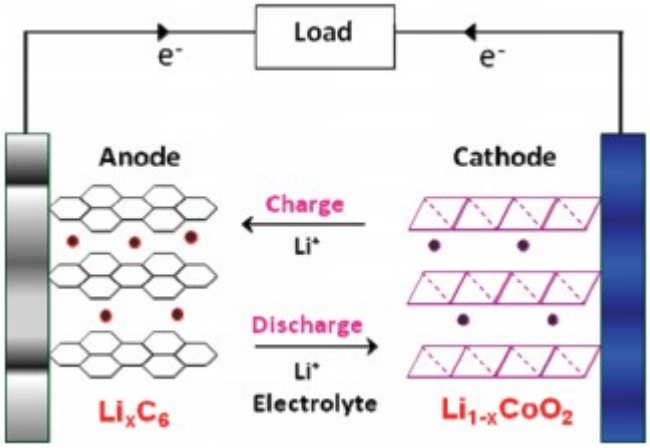

Figure 1.2 illustration of operation mechanism involved in a lithium ion cell consisting of graphite as the anode and layered $LiCoO_2$ as the cathode[2]

In the 1859, the wet cell lead-acid battery, the oldest rechargeable battery, was created by G. Plante. All the batteries applied nowadays are almost variation of the first battery, such as the electrode materials and the electrolyte composition, etc. There are several types of rechargeable batteries (Pb-acid, Ni-Cd and Ni-MH) in the commercial use today with different advantages and the specific application. Pb-acid battery are mostly used in automobile application with low cost and low energy density. Ni-MH batteries hinders their utilization due to fast degradation and poisoning elements. Hence, rechargeable batteries above cannot provide long cycling stability compared to Li-ion battery with organic electrolyte. On the other hand, Li-ion battery offer better electrochemical performance with high potential which is three times of Ni-Cd and Ni-MH batteries[3]. Li-ion batteries do not have to be

completely discharged before recharging, which is commonly operated in Ni-Cd batteries because of the memory effect[4].

Li-ion batteries account for close to 75% of the portable battery market and 20% of the total rechargeable battery market[3]. The market for renewable energy was expected to grow to US$2.6 billion in 2020[5]. Table 1.1 shows the cost of Li-ion batteries remains high for the market compared with other secondary batteries.

Table 1.1 Various types of secondary batteries on a cell level[4]

Technology	Electrolyte	Nominal voltage	Costs (€ /kWh))
Lead acid	H_2SO_4 (4-6 M)	2.0	25-40
Nickel cadmium	KOH (4.5-7 M)	1.2	200-500
Nickel metal hydride	KOH (4.5-7 M)	1.2	275-550 600 (HEV)
Lithium ion ($LiFePO_4$)	Li salt dissolved in organic electrolyte	3.4	200-500 400-800 (HEV)

1.2 Aqueous Rechargeable Lithium-ion Battery (ARLB)

1.2.1 Aqueous electrolytes

The electrolyte, the key point to study on, plays a critical role in keeping electrochemical stability and acting as ion conducting medium and driving electrons to flow via electrodes and external circuit. In the organic electrolytes, only a limited amounts of lithium salts dissolved in the organic solvents with low ionic conductivity. The traditional organic electrolyte, $LiPF_6$ dissolved in the mix solution of ethylene

and dimethyl carbonate, (EC/DMC), can keep the stable electrochemical window at 4 V, which support a large scale of potential difference between cathode and anode and high energy density. However, the state-of-the-state organic electrolyte also takes flammable organic solvents, chemical toxicity, high cost and environmental pollution into account. Besides, the organic electrolyte is moisture/oxygen-dependable, which limits its manufacturing.

Beck and Ruetschi highlighted the "Three E" criteria, namely, energy, economic and environments to optimize current energy storage system[6]. Based on aforementioned organic electrolyte issues, aqueous electrolytes can address all the challenges due to non-flammable and non-toxic nature with low cost and high safety. In 1995, aqueous rechargeable lithium-ion battery (ARLB) was first introduced to public with the use of lithium manganese oxide ($LiMn_2O_4$) and vanadium oxide (VO_2) in the solution of lithium nitrate ($LiNO_3$)[7]. The "rocking chair" concept was also applied in the aqueous oxide which Li-ion can intercalate and de-intercalate from the host.

1.2.2 Electrochemical stability window of aqueous electrolytes

However, the narrow electrochemical window (1.23 V) limits aqueous electrolyte development, which shorten the potential difference of cathode and anode and decrease the diversity of choosing materials to achieve high energy density. To allow the reversible intercalation/de-intercalation of Li-ion, it is important to use two different intercalation compounds in order to avoid water decomposition. When the potential difference of system reaches to 1.23 V, pure water will be decomposed into hydrogen and oxygen gas. At PH=7, its cathodic and anodic limits are located at 2.62

V and 3.85 V versus Li^+/Li, respectively. Most of materials of LIB do not fit in this narrow electrochemical window, except $LiFePO_4$ (3.5 V), VO_2 (2.79 V), $LiTi_2(PO_4)_3$ (2.70V)[8]. This main issue makes aqueous battery only commercially used in low energy density. But this limit can be expanded due to the kinetic effect[9]. Recently, the "water-in-salt" electrolytes (WiSE) provides >3.0V electrochemical window and enriches aqueous batteries with energy densities as high as $200Wh.kg^{-1}$ [3]. Thus, the cathodic and anodic limits are located ~1.7 V and ~4.90 V versus Li. More recently, the electrochemical window of aqueous gel-WiSE electrolytes break the limiting window of 4.0 V when adding a thing coating of gel on the anode to exclude water molecule at the anode surface before SEI forms in the WiSE[8].

1.2.3 Advantages and disadvantages of aqueous electrolytes

For organic LIBs, the cost of organic electrolytes and separator take up the main cost of battery manufacturing. In addition, complicated fabrication process of the Li-ion battery with organic electrolytes requires avoiding moisture, which add its cost. Here, aqueous electrolytes can replace the expensive salts such as $LiPF_6$ with a cheap salt such as LiCl, Li_2SO_4 and eliminate the use of glove box since the ARLB can be fabricated in the moisture and oxygen system.

Besides, safety concerns regarding Li-ion battery attract consumer because numerous fire and explosion in electrical vehicles and mobile phones. Overcharging, overheating and short circuit cause considerable safety issues. When the temperature reaches to 90-120 ℃, combustible gas will be released due to the side reactions. As the temperature reaches to 130 ℃, positive materials will start to decompose and oxygen will be released. When increasing to 200 ℃, electrolytes will decompose into

more combustible gas. However, aqueous electrolytes become a good candidate to address this problem. Water with high thermal capacitance can absorb much heat. For large capacity battery modules, a good cooling system of aqueous electrolyte contacting with electrode is achieved.

The high ionic conductivity of aqueous electrolytes plays an important role in good rate capability and high reversibility. Aqueous solution can offer an incredible ionic conductivity (10^{-1} $S.cm^{-1}$), two order magnitudes higher than the organic electrolytes (10^{-3}-10^{-2} $S.cm^{-1}$), polymer electrolytes (10^{-7}-10^{-3} $S.cm^{-1}$) and inorganic solid electrolytes (10^{-7}-10^{-2} $S.cm^{-1}$)[4]. Furthermore, the activation energy for the Li-ion transfer at electrode (23-25 $kJ.mol^{-1}$) in aqueous electrolytes is much lower than the activation energy in organic electrolytes, suggesting the fast transporting of Li^+ ions from/into electrodes[10].

However, electrochemical performance of aqueous electrolytes depends on concentration, pH and oxygen and additives in the electrolytes. Following Kohlrausch law, the ionic conductivity increases with concentration increasing[11]. But when concentration reaches to saturation point, where numerous ions prevent electricity to flow, causing the decrease of conductivity. Meanwhile, the salts tend to be molecular form instead of ionic form in the solvent[4]. Besides, the voltage plateau was enhanced with the increased concentration, while it did not change much[12]. Electrode materials may exhibit different stability behavior under different pH values of aqueous solution. For the stability of $LiFePO_4$, Porcher et al. found that in the high acidic and basic conditions, there is an increase of dissolved Li^+ and PO_4^{3-}, respectively[13]. Besides,

dissolved O_2 and OH^- ions in the aqueous solution deteriorate polarization and chemical resistance responsible for the capacity fading.

1.3 Superionic electrolytes

Superionic conductor is a type pf exceptionally high value of ionic conductivity (~1ohm.cm^{-1}). Especially, the cubic-structured compounds (A_2BX_4) are impressive lithium conductors[14]. The compound of stoichiometry A_2BX_4 has unoccupied sites in the spinel structure, which is potential to lithium ion diffusion. Tenary lithium chlorides Li_2MCl_4 belong to these family[15]. The spinel type of tenary lithium chlorides Li_2MCl_4 (M=Cr, Mn, Fe, Mg), as the fast lithium ion conductors, has been researched for many years[14]. Ternary lithium and sodium chlorides crystalline such as Li_2ZnCl_4, Na_2CoCl_4, and Na_2MgCl_4, different structure to spinel chlorides, are also fast ionic conductors In an inverse spinel type structure (space group Fd-3m) of Li_2MCl_4 (M=Mg, Mn, Ti, Cd, Fe, Co, Cr and Zn), tetrahedral coordinated lithium ions diffuse via empty octahedral 16d sites. The mechanism of conductivity is an interstitial diffusion of tetrahedrally coordinated lithium ions (8a site) via octahedral interstitial 16d[14]. The ionic conductivity increase with increasing temperature because of an increasing of disorder of lithium ions to these empty octahedral sites. The chloride spinel have a high conductivity of ~0.1 S.cm^{-1} at 400 ℃ and the highest conductivity of 0.32 S.cm^{-1} is reported by Li_2CdCl_4[16].

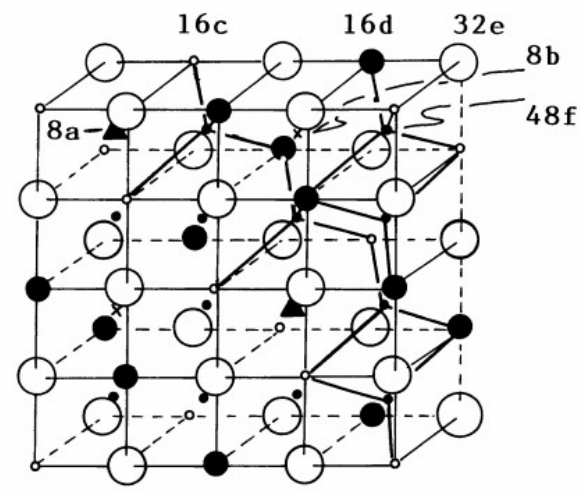

Figure 1.3 Spinel structure of Li_2ZnCl_4[17] The interstitial sites and the ionic conduction pathway are indicated

1.4 Rechargeable Zinc Battery

1.4.1 Advantages of zinc battery

Energy storage plays a predominant role in the everlastingly developing world. Nowadays, energy storage is being optimized to high capacity, fast charge/discharge capability, safety and low cost. Energy storage covers electric vehicles, consumer electronic and military demands, etc. Aqueous rechargeable batteries have advantage over their organic counterparts, when safety, ionic conductivity and cost are taken into account. Lead-acid and nickel-metal (e.g., iron, zinc and cadmium) aqueous batteries are commercially applied in the specific fields[18]. However, they are still limited to find one kind of battery with high energy density and power, good cycle life, non-environmental pollution and safety. Thus, it cannot attract strong interest from researchers.

In the rechargeable batteries, Zinc can be used as an ideal anode material because of excellent thermodynamic properties and large capacity (820 $mAh.g^{-1}$) and low redox potential (-0.76 V vs. SHE), high conductivity, nontoxicity and easy handling. Besides, low cost, safety, abundance and environmental friendly property of zinc attracts attention, compared to lithium, lead and cadmimum. Thus, Zinc has been extensively applied as an active material for negative electrode in zinc-alkaline and zinc-air batteries, as well as acid PH flow cells[19]. Besides, Zn shows a high reversibility and stability. After >500 cycles, the Zn plated on the substrates still exhibits a dense and dendrite-free morphology in a Zn/Zn symmetric cell with HCZE (1 m Zn(TFSI)2 + 20 m LiTFSI)[20]. Another interesting point of ZIBs is a nontoxic, low cost aqueous electrolyte. As is well-known, alkaline such as Ni-Cd, Ni-MH batteries and acid such as lead-acid battery are commonly used with high corrosion. More importantly, ZIB shows high safety according previous findings. Thus, the components of ZIB such as electrolyte, zinc anode, are nontoxic, low cost, safe and abundant for promising commercialization. However, there are still three main issues limiting zinc ion battery development ：surface passivation and electrolytes which do not accept and donate protons and suitable cathodes as intercalaction hosts for Zn^{2+} ions.

1.4.2 Challenges for development of zinc battery

Kang and coworkers have researched four types of MnO_2 as active materials for Zn^{2+} ions intercalation and showed excellent electrochemical performance of α-MnO_2[18]. Liu et al. synthesized the cathodes of zinc hexacyanoferrate (ZnCHF) for

zinc ion battery with energy density of 100 $Wh.kg^{-1}$ and specific charge retention of 76% after 100 cycles.

Zhang et al. proposed an aqueous cheap and environmental-friendly battery with metallic zinc and $Na_{0.95}MnO_2$ in the electrolyte of mixing $Zn(CH_3COO)_2/CH_3COONa$. Although the system does not have a high energy density (78 $W.kg^{-1}$), only 8% capacity lose occurs after 1000 cycles at 4C. In the charging/discharging, zinc ion cannot intercalate into MnO_2 and the intercalation/de-intercalation of Na^+ takes up the reaction in the positive electrode. Zinc can be dissolved and deposited on the negative electrode in the charging/discharging[21].

Rafael et al. created an innovative zinc-ion battery based on copper hexacyanoferrrate (CuCHF) and zinc foil in the electrolyte of zinc sulfate with high voltage of 1.73 V. It makes zinc-ion battery's cyclability, energy values and rate capability reach the level of lithium-ion organic battery based on LiFePO4. Researchers also studied on the effects of hydrogen evolution and zinc ion intercalation on the performance of zinc ion battery. They concluded that the specific states such as PH=6 or low concentration of zinc can favor the zinc morphology and avoid the formation of dendrites[19].

Among aqueous metal-ion batteries, many metal-ion batteries except lithium ion battery are restricted in the electrode materials for the insertion and extraction of metal ion. Because of the limits of intercalation host for Zn^{2+}, the selection of cathode materials actually focus on lithium and sodium ion batteries to form some hybrid aqueous systems with zinc anodes. Zhang [22] and coworkers have researched the LiMn2O4 as cathode in the zinc ion battery to discuss the working mechanism and

found Zn|CH_3COOLI+$Zn(CH_3COO)_2$|$LiMn_2O_4$ has high capacity and good rate performance above 20C.

1.4.3 Hybrid battery of LiFePO4/Zn

The hybrid battery is composed of a metal as anode and a de-intercalation/ intercalation materials as cathode to operate on the rocking-chair model such as sodium-ion battery, fluorine-ion battery[23]. The electrolyte is composed of two kind of ions from cathode and anode to mix. Figure 1.4 show some promising materials for cathodes and anodes. The middle area covers materials in the aqueous battery. $LiFePO_4$ has no phase change, which shows a good cycling and stable performance for hybrid battery. For anodes, Fe, Co and Ni can be as candidates. However, Zn (-0.76 V vs. SHE) can supply a higher output voltage (-0.76V-(-0.41V)=1.2V) than that of Ni (-0.257V), Co (-0.277V) and Fe (-0.447V). And Zn is also has low cost, stability, safety and no toxicity as said before. The specific capacity of $LiFePO_4$ and Zn is 170 $mAh.g^{-1}$ and 820 $mAh.g^{-1}$.

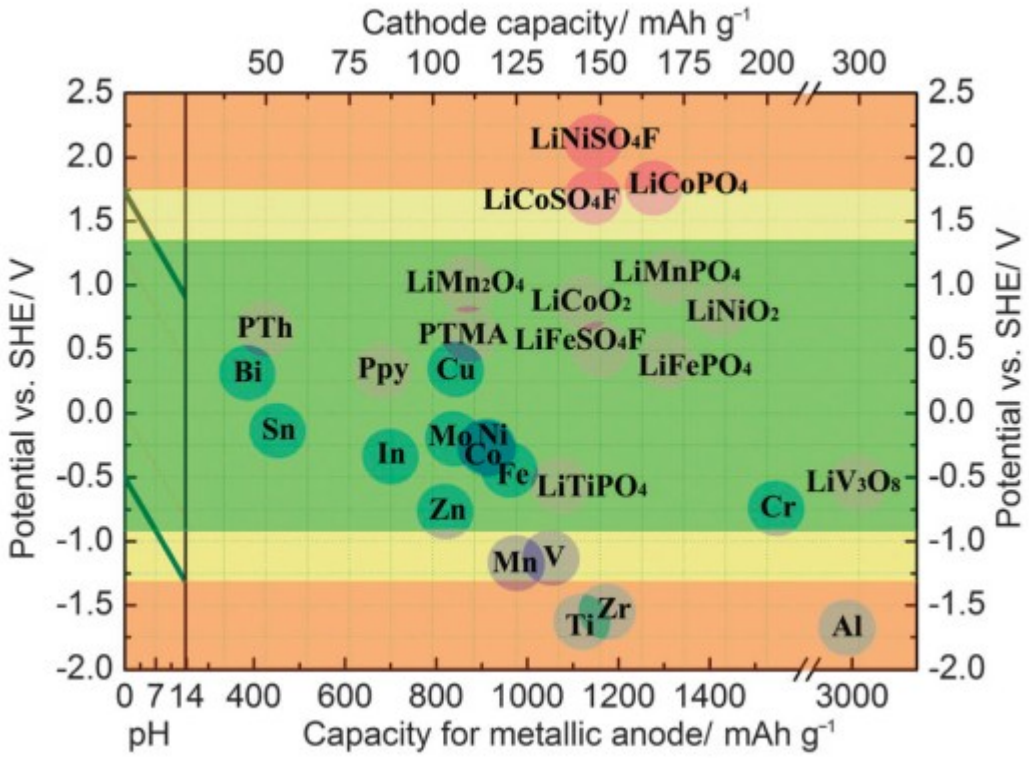

Figure 1.4 Cathode And anode candidates for the hybrid system, aqueous electrochemical window at green[24]

Zhang and coworkers has found two kinds of ions work with each other to run $LiFePO_4$/Zn hybrid battery with long cycle life and satisfying rate performance. When the battery is charged, the Li^+ de-intercalates from $FePO_4$ and dissolves into the electrolyte. At the same time, Zn^{2+} is reduced and deposit on the surface of Zn (anode). When it is discharged, the Zn on the anode lose electron to dissolve in the electrolyte and electron from the outside circuit take up Li^+ from electrolyte. It is evident that the concentration of Li^+ and Zn^{2+} fluctuate continuously during the charging /discharging process. Thus, this system of $LiFePO_4$/Zn can offer a high output voltage about 1.2V with high capacity, rate capability and cyclability,

indicating promising candidate for electric vehicles and other applications. Thus, this work proposed the innovative concept of aqueous Li^+/Zn^{2+} mixed-ion electrolytes to construct rechargeable $LiFePO_4$/Zn hybrid batteries at the first time.

Cathode:

$$LiFePO_4 == Li^+ + e^- + FePO_4$$

Anode:

$$Zn^{2+} + 2e^- == Zn$$

Overall reaction:

$$LiFePO_4 + 0.5Zn^{2+} == Li^+ + 0.5Zn + FePO_4$$

1.5 Cathode Material: $LiFePO_4$ at extreme temperature

1.5.1 Effects of high temperature on batteries

With increasingly developing society, batteries are required to operate under extreme conditions. For some NASA's planetary application and military needs, rechargeable lithium battery with high energy density operating at extreme low temperature is required urgently. However, Li-ion battery, the common battery in the commercial application, is limited to room temperature due to the thermal fluctuation. The traditional efforts make the Li-ion battery operate at low (< 20℃) or high (> 60℃). The performance and safety of battery in the extreme temperatures depends on the competency of electrolytes, current collectors and separators, properties of cathodes and anode materials[25].

In the high temperature, cathode materials are susceptible to irreversible phase transition[25]. Moreover, the side reaction on the interface of cathode and electrolyte

accelerates the damage of structure under high temperature, which increases metal dissolution and oxygen evolution. All the disadvantages under high temperature cause the performance degradation, such as active materials losing and instability of structure. Besides, the thermal stability of electrolyte decays as well due to the reaction of electrodes with flammable electrolyte, which threats the safety issues.

1.5.2 Effects of low temperature on batteries

Despite the limited research on the mechanisms of decreased performance of LIBs at low temperature. However, the main issue focuses on intrinsic kinetic constraints, such as slow charge transfer and lithium ion diffusivity. Main factors influencing the performance at low temperature are attributed to the electrolyte and interface between electrolyte and electrode. Various research on modifying electrolyte properties, but the effect does not reach satisfaction. Braja K. Mandal et al. adjusted the ration of EC, EMC, DMC and PC with 0.9 M LiTFSI to achieve a promising electrolyte in the cell of $LiNi_{0.8}Co_{0.2}O_2$/graphite which can operate in the range of -30 to 70 ℃[26]. However, the conductivity is just close to 2.0 $mS.cm^{-1}$ at -40 ℃. Kebin Chen et al. studied on LMO/LTO (lithium manganese oxide/lithium titanate) lithium ion battery with three electrolytes at -30 ℃[27]. It showed that esters, such as ethyl acetate (EA), methyl butyrate (MB) with low melting point and low viscosities improved the electrochemical performance at low temperature. However, the conductivity of the best electrolyte, 1M $LiPF_6$ in EC: EMC: EA (1:5:4 vol %), is 2 $mS.cm^{-1}$ at -20℃. Thus, how to improve the activity of lithium ion diffusion and internal resistance is the point of performance at low temperature. Fig 1.5 summarizes

the operating temperature and energy density for some commercial rechargeable batteries.

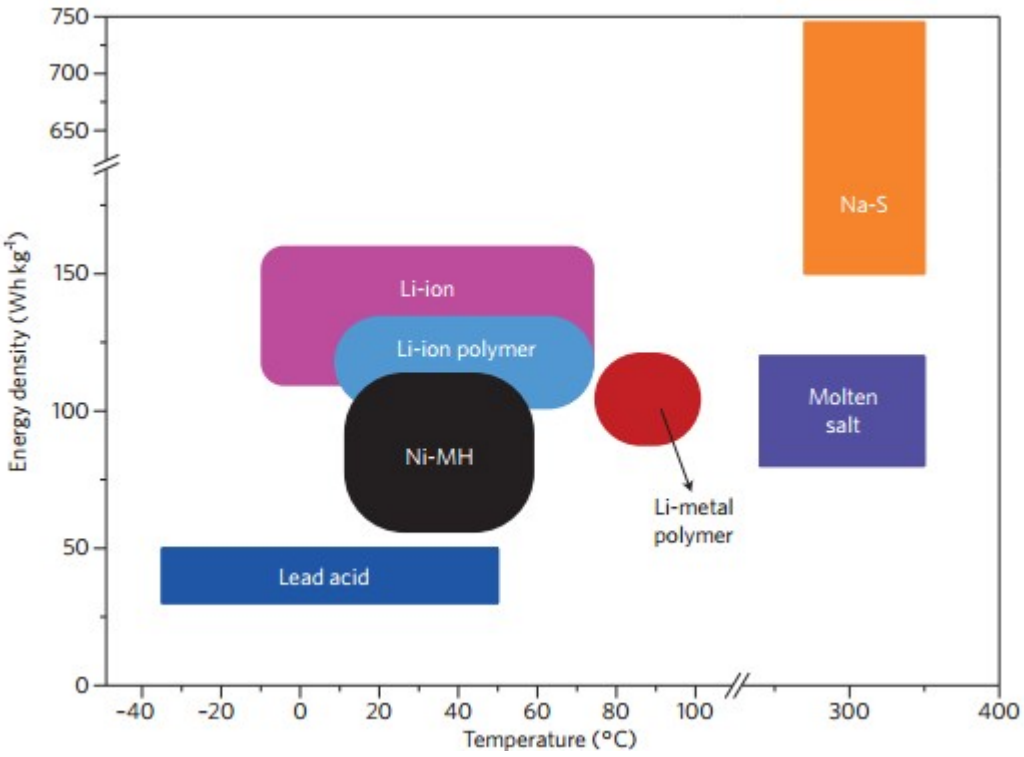

Figure 1.5 Summary of energy densities and temperature windows of commercially rechargeable batteries[25].

1.5.3 LiFePO4 at high temperature

Lithium iron phosphate with an olivine-type structure has been a candidate of cathode materials for Li-ion batteries because of low cost, chemical stability and thermal stability and excellent safety. However, $LiFePO_4$ is an insulating material which limit its rate capability. The development of $LifePO_4$ mainly focuses on how to increase the electronic conductivity of $LiFePO_4$.

Of the known cathode structures, general application in the high temperature give priority to the phosphate and lithium iron phosphate ($LiFePO_4$) due to the high thermal and structural stability. PO_4^{3-} is unlike other metals oxides in the battery such as $LiMn_2O_4$, $LiCoO_2$, which does not produce oxygen in the high temperature. Secondly, the volume change is small between $LiFePO_4/FePO_4^-$. However, the cycling stability of the olivine is not good as reported at high temperature, which is an obstacle for a stable and low cost cathode materials. Even at 37℃, the carbon-coated $LiFePO_4$ capacity loses ~40% of original capacity for 100 cycles in $LiPF_6$/EC: DEC (3:7). At 55℃, the capacity loses dramatically ~70% of original one for 100 cycles, owing to an amount of iron ion dissolution and the impedance increase[28]. Coating of carbon, polymer or metal oxide is the general approach to increase its electronic conductivity. Chang and his workers found TiO_2 coating directly prevents the contact between $LiFePO_4$ and electrolyte and reduces the cathode erosion upon cycling in the system of $LiFePO_4$/Li. Their team also found carbon as anode has a deteriorating effect on cycling stability because of SEI formation consumption[29]. It indicates $LiFePO_4$ has a major issue with cycling at elevated temperature

1.5.4 LiFePO4 at low temperature

In the low temperature, the main point to be solved is the slow charge transfer and lithium ion diffusivity. $LiFePO_4$ has >300% higher charge-transfer resistance at -20 ℃ than at room temperature[25], in addition to the difficulty of lithium ion diffusion Besides, electrochemical performance of LIB is also affected by the high grain-boundary resistance and Li^+ ion diffusion inside the cathode. Generally, smaller particle size and coating conductive polymer or carbon can alleviate effectively the

resistance from lithium ion diffusion and inter-grain. Zhang and his coworkers doped La^{3+} and Mg^{2+} into $LiFePO_4$ and coated carbon aerogel on $LiFePO_4$ to improve the electrochemical performance of the composite at low temperature with high rates[30]. Thus, how to improve poor ionic and electronic conductivities of $LiFePO_4$ is still extensively studied to address the electrochemical problems at low temperature.

1.6 Poly (3, 4-rthylenediocythiophene)

1.6.1 Application of PEDOT in batteries

Poly (3, 4-rthylenediocythiophene) or PEDOT is a 'sky-blue' conducting polymer based on EDOT. PEDOT is extensively researched because of the transparence, flexibility, easy polymerization[31]. The prior advantage of PEDOT is high electronic conductivity and more chemical stability than most other conducting polymer. Thus, PEDOT is a highly concerned materials with various applications in batteries, supercapacitors, electronics and optics.

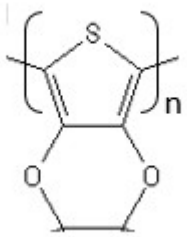

Figure 1.6 Structure of PEDOT

Liu and his coworkers coated PEDOT on $LiNi_{1/3}Co_{1/3}Mn_{1/3}O_2$ to improve rate and cycle performance[32]. They also believed that an appropriate thickness of coating is curial to electrochemical performance and PEDOT can alleviate surface

polarization and prevent side-reactions at the interface between electrolyte and electrode.

Ma and his colleagues created a novel hierarchical structure of 3DOM FeF_3 coated with PEDOT which increase capacity under high current density at room temperature[33]. At low temperature (10 C°), capacity still maintained at 90 $mAh.g^{-1}$ and no obvious capacity degradation was observed. However, at the high temperature of 55C°, the cycling stability decreased distinctly.

Yao and his coworkers coated PEDOT on the anode of Silicon nanowires improves cycling to increase the capacity retention from 30% to 80% over bare nanowires after 100 cycle, stemming from the mechanical integrity of Si materials and electrical connections between NWs[34].

Many polymers with high conducting and mechanical flexibility, such as PPy and PEDOT, can show larger capacities because of the increased surface contact, improved lithium diffusion pathway[35]. The aforementioned researches indicates PEDOT shows an excellent electrochemical behavior, especially in improving rate and cycle performance at the room temperature, due to its high electrical conductivity and good electrochemical stability. Besides, PEDOT is one of the few conjugated polymers which is both p- and n-dopable. Its low oxidation potential make it easily being oxidized[36]. Upon oxidation or reduction, the electrochemical p-doping (n-doping) conducting PEDOT will increase electronic conductivity and change spectral changes in structural transition. Besides, some researches shows PEDOT has comparable capacity. Zhang and his coworker firstly applied PEDOT as the active cathode materials in 1M $LiN(CF_3SO_2)_2$/1,2-dimethoxyethan/1,3-dioxolane (1:2 by

weight) solution[37]. The cell shows a high capacity of 691 $mAh.g^{-1}$ at the 1st cycle and remains 333 $mAh.g^{-1}$ after 44 cycles with 2.2V discharging plateau vs. Li/Li^{+}. They also believed the multi-electron electrode reaction of PEDOT affords such a high capacity (theoretical capacity 752 $mAh.g^{-1}$).

1.6.2 The Synthesis of PEDOT

3, 4-ethylenedioxythiophene (EDOT) is the monomer which can be polymerized produce the polymer PEDOT by either chemical or electrochemical method. The synthesis of PEDOT proceeds with a reaction stoichiometry of 2.33 moles of electrons per mole of EDOT[38]. The polymerization can be easily carried out in aqueous solution and room temperature while the low solubility of PEDOT in this solvent. The yield of PEDOT depends on the time of reaction and the amount of oxidant. Conductivity of PEDOT decrease and yield of PEDOT increases with increasing temperature[38]. $FeCl_3$, $Ce(SO_4)_2$,$(NH_4)_2S_2O_8$ and $(NH_4)_2Ce(NO_3)_6$ are common oxidants to polymerize EDOT[38, 39].

Chapter 2: Theory and Experiment

2.1Material Synthesis and Preparation of Electrolytes

2.1.1 Different amounts of PEDOT coating on LiFePO4

Firstly, $LiFePO_4$ (MTI, KJ $LiFePO_4$) was added into 250ml flask. Deionized Water (70ml) and Methanol (10ml) was added into the solution. The suspension was treated in ultrasonic cleaner for 2 hours. Secondly, 0.1ml EDOT (Aldrich, 97%) was added to the solution and then stirred vigorously for 10min. 0.2g $(NH_4)_2S_2O_8$ (Sigma-Aldrich, ≥98 %) dissolved in Deionized Water (10ml) was added to the solution. The mixture solution was stirred for 48h in room temperature. Finally, the solution was washed several times with water ethanol, and dried overnight at 80 ℃ in vacuum to get $LiFePO_4$@PEDOT. For Brevity, the PEDOT-coated $LiFePO_4$ powder will hereafter be abbreviated as c-LFP1, 2, 3 according to the loading of coating, while the uncoated $LiFePO_4$ as u-LFP. The ratio of $LiFePO_4$ and EDOT which were added to reactors as the table below

Table 2.1 Three ratio of $LeFePO_4$ and EDOT in the synthesis

	$LiFePO_4$ (mg)	**EDOT (ml)**
c-LFP1	500	0.2
c-LFP2	500	0.1
c-LFP3	500	0.05

2.1.2 Electrolytes of Li2ZnCl4.xH2O

LiCl (Sigma-Aldrich, anhydrous, ≥99 %) and $ZnCl_2$ (Alfa Aesar, anhydrous, 98^+ %) were added to 15ml vial and then dissolved in deionized water (molar ratio of LiCl, $ZnCl_2$, H_2O=2:1:6/9/12) different molar ratio. The solution was stirred in the closed vial with strong dissolution heat and then returned to room temperature to get electrolytes of $Li_2ZnCl_4.6H_2O$ (9.12 $mol.kg^{-1}$), $Li_2ZnCl_4.9H_2O$ (7.83 $mol.kg^{-1}$), $Li_2ZnCl_4.12H_2O$ (6.86 $mol.kg^{-1}$).

2.2 Characterization Methods

2.2.1 Electrolytes and powder characterization

To identify $Li_2ZnCl_4.xH_2O$, Raman Spectroscopy and Thermal Gravimetric Analysis (TGA) were performed for the electrolytes. In-situ Raman spectra of $Li_2ZnCl_4.xH_2O$ were collected with a Horiba Jobin Yvon Labram Aramis using a HeNe laser (632.8 nm) between 4000 and 30 cm^{-1}. For this characterization, seven different concentrations of solution and six different ratio of LiCl and ZnCl2 of $Li_2ZnCl_4.9H_2O$ and pure solid powder of LiCl and ZnCl2 were prepared. In the TGA, the different concentration of $Li_2ZnCl_4.xH_2O$ (x=6, 9, 12) and pure water, weighing approximately 15~30mg each, were heated from Room Temperature to 350 ℃ at the heating rate of 4 ℃.min^{-1} in the argon flow of 100 $ml.min^{-1}$ at the balance alumina sample pan, using a TGA SDT Q600 instrument (TA Instruments, USA). For the measurements in the low temperature, all three electrolytes were performed with Differential Scanning Calorimetry (DSC). A very small amount of MCMB was added to each sample. Each sample hermetically sealed in the aluminum pan with lid,

weighing approximately 15~30mg, was cooled from RT to -145°C at the rate of -5 °C.min^{-1} and then was heated to RT at the rate of 2 °C.min^{-1}. The weight of PEDOT coated on $LiFePO_4$ was also measured by TGA analysis, which heating c-LFP2, pure PEDOT and pure $LiFePO_4$ (weighing 10~15mg) respectively from room temperature to 800 ℃ at the heat rate of 4℃.min^{-1} in air flow of 80 ml.min^{-1}.

X-ray diffraction (XRD) measurements were performed for the dehydrated Li_2ZnCl_4 powder (heating $Li_2ZnCl_4.9H_2O$ at 205°C for 24 hours). The crystal structure of Li_2ZnCl_4 powder were achieved by powder XRD using a CuK_α radiation source on a D8 Advance with LynxEye and SolX (Bruker AXS, WI, USA) in the 2θ range of 5°to 90°. The crystalline phase analysis was achieved from the relative intensities of reflection from XRD via JADE 6.5 software.

The morphology and structure of the tested c-LFP2 was observed with transmission electron microscopy (TEM, JEM 2100LaB6, 200 keV). The cathode of c-LFP2 was dissolved into PEDOT-coated $LiFePO_4$, Carbon black and PTFE and suspended in the ethanol in the ultrasonicator for 3 hours.

2.3 Electrochemical Measurement Technology

2.3.1 Cyclic Voltammetry

The Cyclic Voltammetry (CV) is a popular used technology of electrochemical studies, useful for obtaining qualitative information such as complicated electrode reactions, intermediates in oxidation-reduction reaction and the reversibility of reaction. Oxidation and reduction reaction in turn happen on the electrode when voltage is swept between upper limit and lower limit at a stable rate. CV depends on

the scan rate of voltage, the rate of the electron transfer reaction and the chemical reactivity of active materials. Three electrodes system is used in the cyclic voltammetry. The potential of working electrodes versus a reference electrode is measured and the resulting potential generates a signal such as figure. In the forward scan, the potential sweep negatively from a greater potential to a lower potential. V_2 is the switching potential where the voltage is enough to oxidation and reduction reaction. The backward scan sweep from V_2 to V_1. A cyclic voltammetry figure is achieved by relationship of current measured on the working electrode and potential. Figure 2.1 shows a cyclic voltammetry of single reduction and oxidation. A reduction occurs at c and an oxidation occurs at a. i_p^c is called cathodic current and E_p^c is called the cathodic peak potential. When potential reaches E_p^c, all the substrate on the working electrode are reduced. E_p^a is the anodic peak and i_p^a is the anodic current. All the substrates on the working electrode are oxidized. In this measurement,

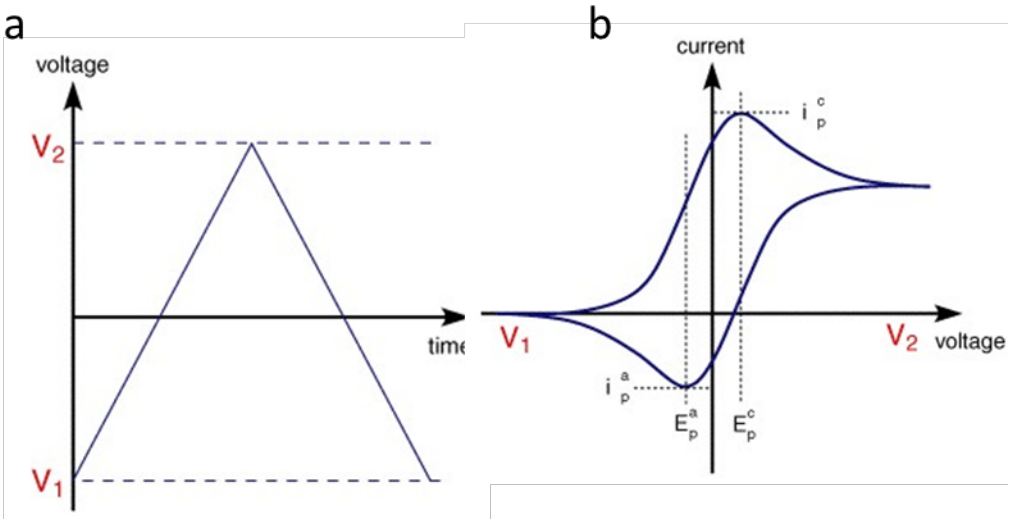

Fig 2.1 (a) The excitation signal of CV. (b) CV curve with the potential versus reference electrode[40]

Ag/AgCl electrode is the reference electrode. Activated carbon is the counter electrode. Glassy carbon is the working electrode. The electrolyte was characterized on an electrochemical analyzer (CH Instruments, US).

2.3.2 Electrochemical performance

The electrochemical performance of $LiFePO_4$@PEDOT was measured in a vial which consist of two titanium rods, one with excessive zinc foil (Alfa Aesar, 0.25mm thick, 99.98%) as anode, one with $LiFePO_4$@PEDOT pressed on the titanium grid (Alfa Aesar, 100mesh, 0.05mm). The cathode material is mixed with $LiFePO_4$@PEDOT as active materials, carbon black (Saft) to increasing the conductivity and ploythetrafluoroethylene (PTFE) (Aldrich, 60wt% dispersion in H_2O) as binder of weight ratio: 8:1:1. Because of electrochemical measurement in the high and low temperature, the vial must be sealed to keep the stability of electrolyte.

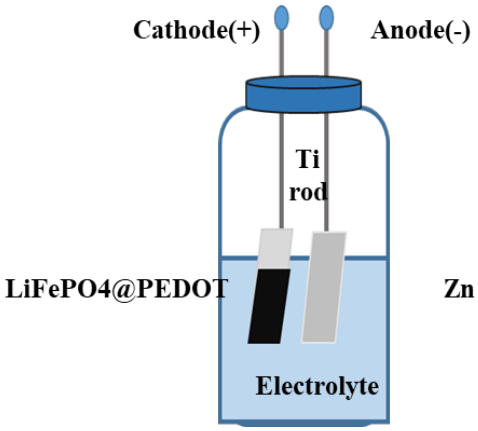

Fig 2.2 Schematic graph of the cell assembled for electrochemical test

The ionic conductivity of the electrolyte can be calculated from the equation below:

$$\sigma = \frac{1}{\rho} = \frac{l}{R * A}$$

where σ is the ionic conductivity of the electrolyte, ρ is the resistivity of material, R is the resistance of material, l is the distance between two flat electrodes and A is the cross-section area of electrodes. Because of the accuracy of measurement of A and l, the standard solution (1413 $\mu S.cm^{-1}$ NaCl conductivity/TDS standard) can be a reference to be measured at first and then calculate the conductivity of electrolyte according the equation below:

$$\frac{\sigma}{\sigma_{standard}} = \frac{\rho_{standard}}{\rho}$$

The conductivity of a solution can be measured by testing the resistance of the solution between two flat electrodes, parallel to each other. The operating frequence is normally in the range of 1-3 kHZ. Here, the ionic conductivity of electrolyte was

measured between two titanium electrodes by an electrochemistry workstation (Gamry instrument) from 300000 Hz to 0.01Hz at different temperature.

Chapter 3: Characterization Discussion and Results

3.1 Raman and XRD Characterization

Sample was prepared by drying the solution of $Li_2ZnCl_4.9H_2O$ at 205 °C for 24 hours. The crystalline reflections with the composition Li_2ZnCl_4 could be indexed according to JCPDS#41-0386. The XRD patterns of the sample shows evident crystalline peaks, indicating the existence of pure Li_2ZnCl_4. Crystal data and structure refinement details of Li_2ZnCl_4 is on the table. The XRD pattern of the phase of Li_2ZnCl_4 was a cubic cell with a cell constant a=10.346 A, with space group Fd3m. Table 3.1 shows unit cell dimensions a [Å], b [Å], c [Å], β [degree], density Q [$g.cm^{-3}$] and mol volumina V_m [$cm^3.mol^{-1}$] of Li_2ZnCl_4

Table 3.1 Structure parameters of Li_2ZnCl_4

Compound	**a**	**b**	**c**	**β**	**Q**	**V_m**
Li_2ZnCl_4	10.346	10.346	10.346	90	2.652	110.74

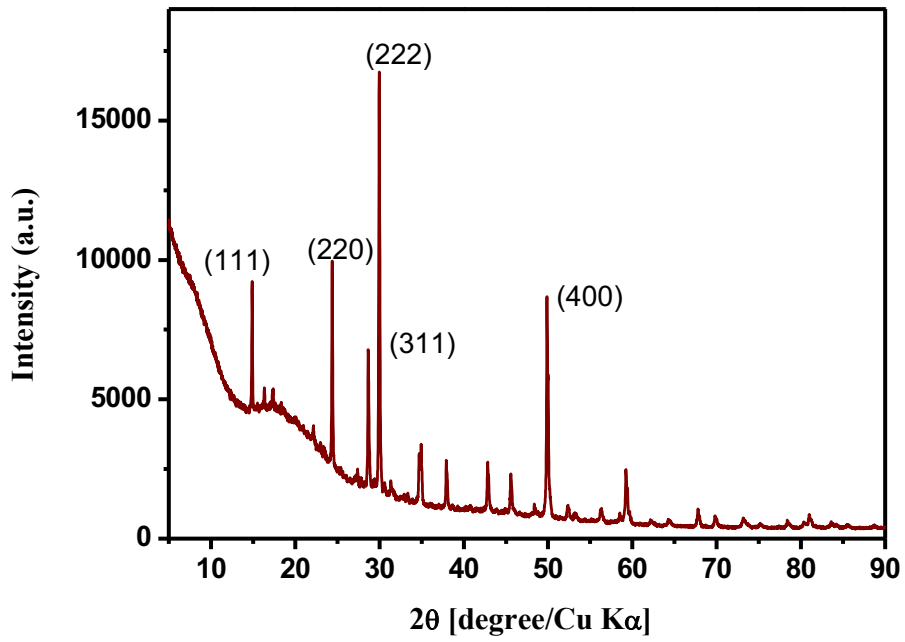

Figure 3.1 XRD pattern of the dehydrated $Li_2ZnCl_4.9H_2O$ sample

Fig 3.2 shows the Raman Spectra measured for six concentrations of $Li_2ZnCl_4.xH_2O$ ((x=6 (9.12 mol.kg^{-1}), 9 (7.83 mol.kg^{-1}), 12(6.86 mol.kg^{-1}), 22.5 (4.79 mol.kg^{-1}), 72 (1.98 mol.kg^{-1}), 156 (0.99 mol.kg^{-1})). When x= 6, 9, 12, 22.5, a broad band centered at 102 cm^{-1} matches well with previous findings[41-43]. In the Raman spectra of aqueous $ZnCl_2$ and $ZnCl_2.3LiCl.15H_2O$ and solid $ZnCl_2$, in which a tetrahedral structure of $ZnCl_4^{2-}$ exists, two tetrahedral bending modes, a υ_4 mode at 117 cm^{-1} and a υ_2 mode at 96 cm^{-1}, are merged into one broad band at ~110 cm^{-1} [41-43]. However, in the liquid state the two modes are broaden and the peak at ~102 cm^{-1} looks like one envelop.

The strongest band at ~282 cm^{-1} excellently agrees with previous results of solid $ZnCl_2$ and glassy $Li_3ZnCl_5.15H_2O$, because of the υ_1 mode of the tetrahedral of $ZnCl_4^{2-}$ [41-43]. The Raman spectra of solid powder of $ZnCl_2$ also shows two peaks at 111 cm^{-1} and 228 cm^{-1}, which indicates the existence of $ZnCl_4^{2-}$ in the solid state. For the comparison of different concentration of Li_2ZnCl_4, when the concentration increases up to 5 $mol.kg^{-1}$ ($Li_2ZnCl_4.22.5H_2O$), the Zn^{2+} and Cl^- aggregate and form the tetrahedral structure of $ZnCl_4$, as found in the Raman studies.

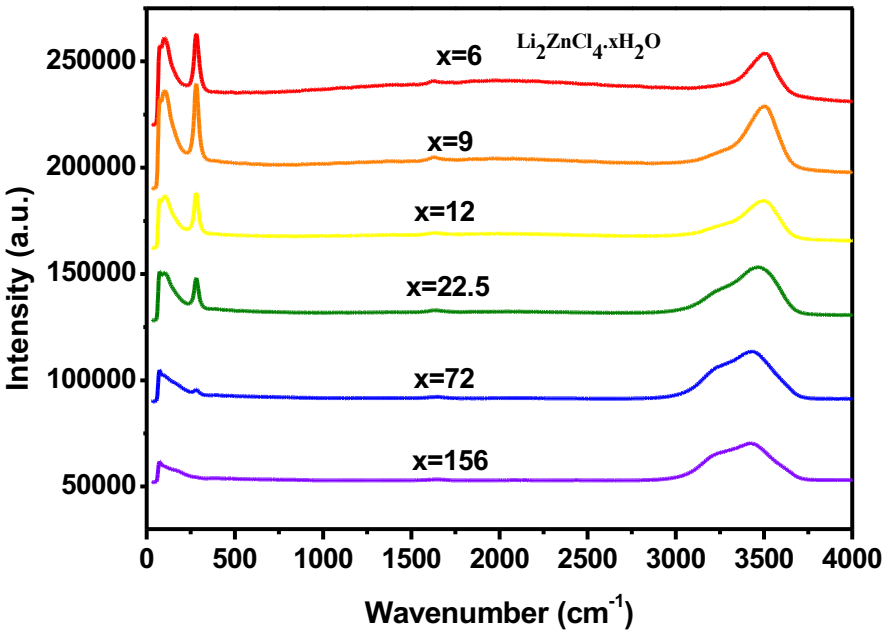

Figure 3.2 Raman spectra of seven different concentration of $Li_2ZnCl_4.xH_2O$ (x=6, 9, 12, 22.5, 72, 156)

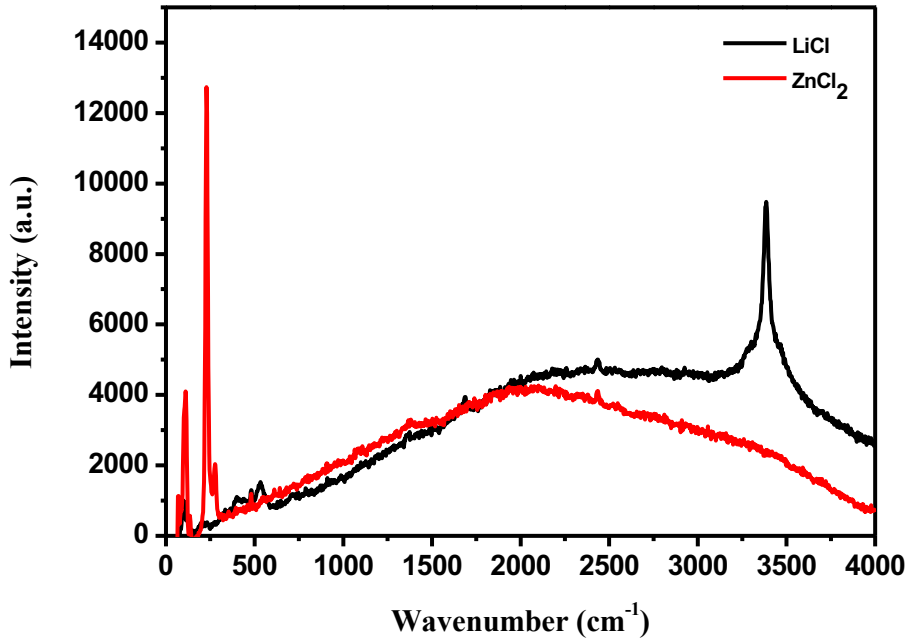

Figure 3.3 Raman spectra of solid $ZnCl_2$ and LiCl powders

Besides, Raman Spectra also measured five solutions with different ratio of lithium and zinc in (2+y) LiCl. $ZnCl_2.9H_2O$ when y=0.4, 0.2, 0, -0.2, -0.4 in Fig 3.4. Raman Spectra indicated $ZnCl_4^{2-}$ exists in all the five solutions which have the moderate deviation to standard ratio of Li^+ and Zn^{2+} (2:1) when they all show the characteristic peaks of $ZnCl_4^{2+}$ at 102 cm^{-1} and 282 cm^{-1}. But electrolyte at acidic and basic conditions have a great effect on the stability of $LiFePO_4$, causing dissolved PO_4^{3-} and the ratio of Zn^{2+} and Li^+ also fluctuate with charging/discharging the cell of $LiFePO_4|Li_2ZnCl_4.9H_2O|Zn$. Thus, the ratio of LiCl: $ZnCl_2$ =2:1, as the electrolytes, is studied in this research, based on the Raman Spectra.

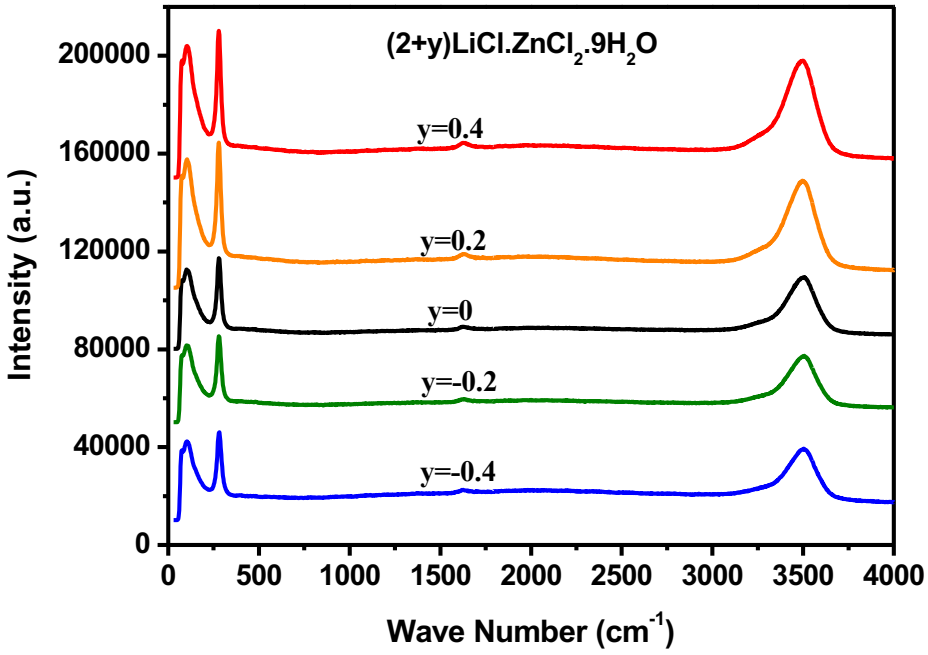

Figure 3.4 Raman Spectra of five solutions of (2+y) $LiCl.ZnCl_2.9H_2O$ (y=0.4, 0.2, 0, -0.2, -0.4)

3.2 Measurement of Ionic Conductivity of $Li_2ZnCl_4.9H_2O$

Figure 3.5 shows the relationship pf ionic conductivities of $Li_2ZnCl_4.9H_2O$ and temperature measured from -75 °C to 80 °C. Ionic conductivity increases with increasing temperature at the linear relationship of log (σ) and 1/T. At room temperature, the conductivity reaches to 0.108 $S.cm^{-1}$. At 70 °C, the extreme operating temperature, the conductivity is 0.207 $S.cm^{-1}$. It was also measured at -70 °C, the conductivity of $Li_2ZnCl_4.9H_2O$ is 1.002 $mS.cm^{-1}$. The ionic conductivity of $Li_2ZnCl_4.9H_2O$ system is two order magnitude higher than that in some organic

electrolytes. The extremely high ionic conductivity of $Li_2ZnCl_4.9H_2O$ system at -75 °C support the feasibility of operating at low temperature.

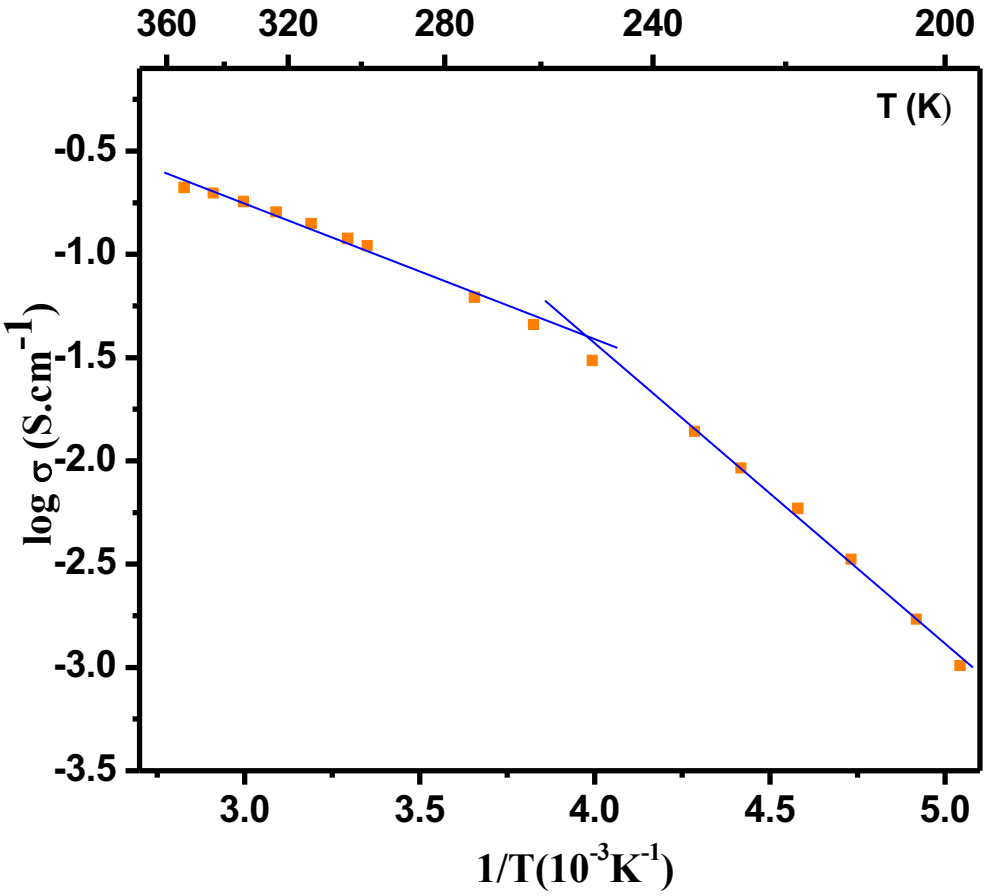

Figure 3.5 Ionic conductivity of $Li_2ZnCl_4.9H_2O$ tested from 80°C to -75°C

3.3 Analysis of Thermal Stability on $Li_2ZnCl_4.xH_2O$

In the TGA curves as Fig 3.6, the y axis is presented as the percentage of $(m-m_{final}) / (m_{inital}-m_{final})$, where m, m_{inital}, m_{final} are the mass, initial mass and final mass, respectively. By normalizing the data in this manner, the DSC-TGA curves can

reflect the water content of $Li_2ZnCl_4.xH_2O$ (x=6, 9, 12) and the percentage of losing water in a clear way. Pure water can be as the calibration and comparison to the electrolytes. In three different concentration of $Li_2ZnCl_4.xH_2O$, they show two distinct weight loss zones from room temperature to 350°C. The first zones, from room temperature to ~145 °C corresponds to losing free water. Compared to pure water, the rate of losing water slow down largely. After the first zone, an amount of water (bound water) was bound in the Li_2ZnCl_4 salt, remaining 13%, 28% and 29% of total water with increasing concentration, respectively. The second zone, after 200 °C corresponds to losing bound water. The ratio of bound water to free water increases with increasing concentration of solution.

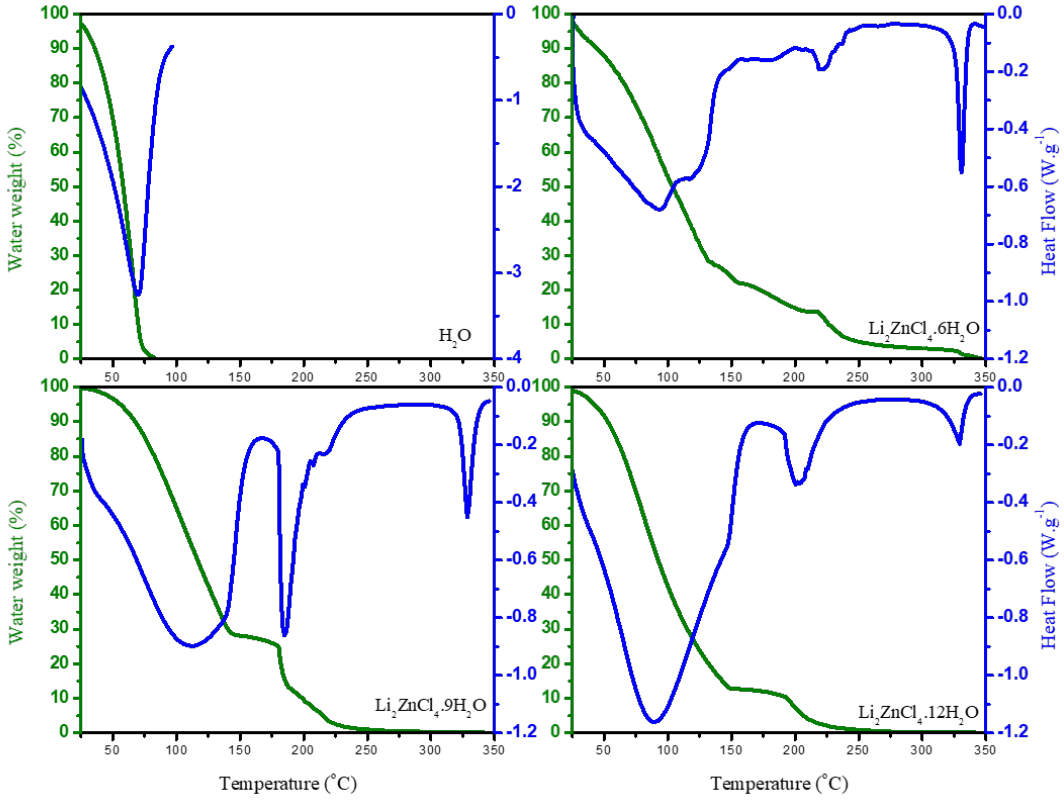

Figure 3.6 DSC-TGA curves of pure water and $Li_2ZnCl_4.x\ H_2O$ (x=6,9,12) heating in argon flow of 100 ml/min at a rate of 5°C /min from 25°C to 350°C. Weight-loss curve (Green) and heat flow curve (Blue).

For DSC curves in the low temperature as shown in Fig 3.7, only $Li_2ZnCl_4.6H_2O$ exhibited precipitation and subsequent melting points at B (-74°C) and C (-11°C), respectively. However, there is no phase transformation for $Li_2ZnCl_4.9H_2O$ and $Li_2ZnCl_4.12H_2O$, which show a huge range of stable state. The three electrolytes were supercooled to their glass transition temperature T_g at A (-99.5°C), B (-115 °C) and C (-120 °C), respectively, which are of a regular order. Thus, they should resist

crystallization strongly. However, it is not sure if the effect of Zn^{2+} solvation on the DSC curves.

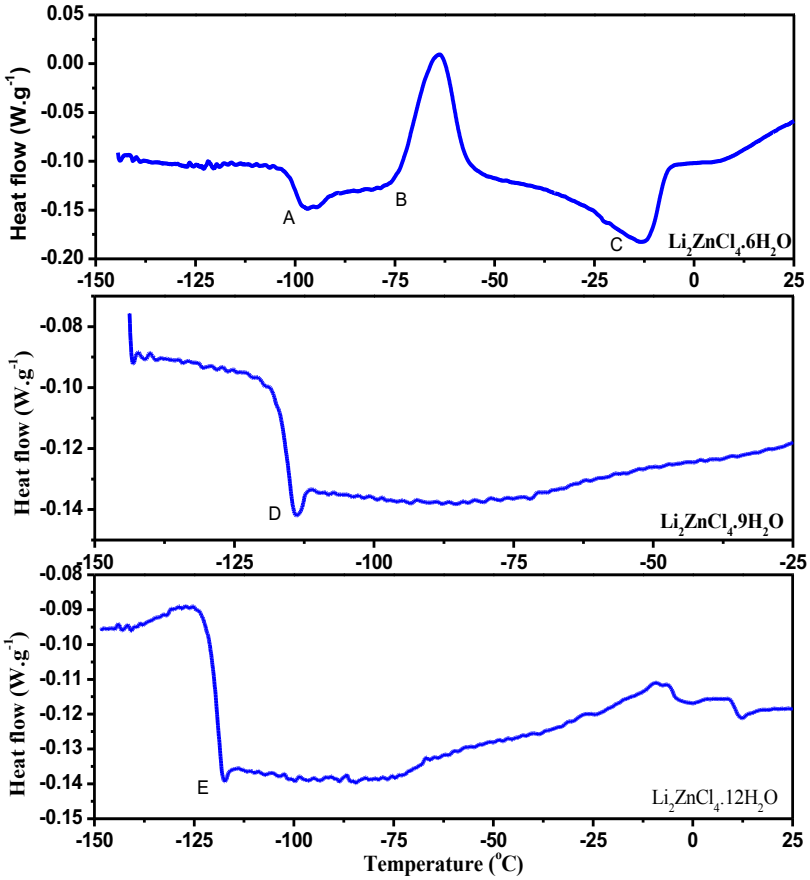

Figure 3.7 DSC curves of $Li_2ZnCl_4.x\ H_2O$ (x=6, 9, 12), cooling at a rate of 5°C /min from RT to -145 °C.

3.4 TEM Characterization of PEDOT-coated $LiFePO_4$

TEM was conducted on the powder of c-LFP2 with micro-sized particle before and after testing. For the sample c-LFP2, a coarse surface with a coating layer about 50 nm can be seen clearly in Fig 3.8. After testing, a 50nm layer can be still observed.

It confirms that PEDOT exists stably on the particle surface. By TGA analysis and calculation, ~8.6 wt. % PEDOT was coated on the $LiFePO_4$.

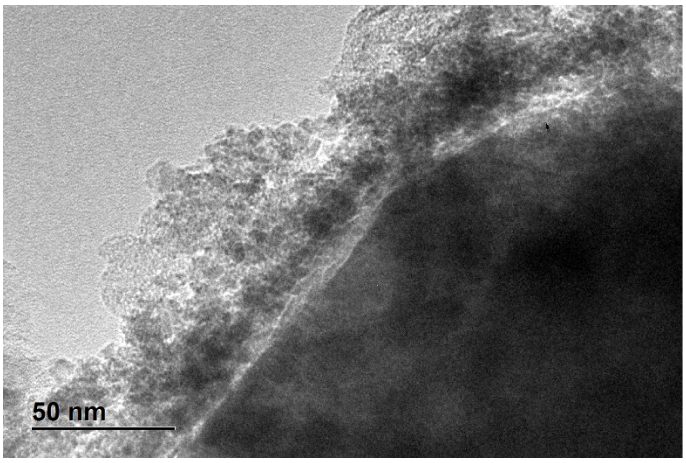

Fig 3.8 TEM image of the tested c-LFP2 sample

3.5 Cyclic Voltammetry for Electrochemical Stability Window

The CV test was measured in the same cell as the cell in the electrochemical test at the room temperature. Ag/AgCl electrode (3.2 V vs. Li/Li^+) is the reference electrode. The measurement was scanned between 4.5 V to 2.2 V (vs. Li/Li^+) at the scanning rate of 5 mV/s. Anodic peak at ~4.5V stands for production of Cl_2 at high voltage according to the standard reduction potential. The cathodic peak at ~2.2 V stands for the Zn plating at low temperature. This CV test shows that the Li_2ZnCl_4 .$9H_2O$ show a huge electrochemical stable window of 2.3V. Although it cannot reach the electrochemical stable window of >3.0 V, the cathodic limit reach

the anode of zinc deposition and the anodic limit reach to a large scale of various cathode materials, such as $LiFePO_4$ (3.50V), $LiMnO_2$ (4.1V), $LiNi_{1/3}Mn_{1/3}O_2$ (4.2 V).

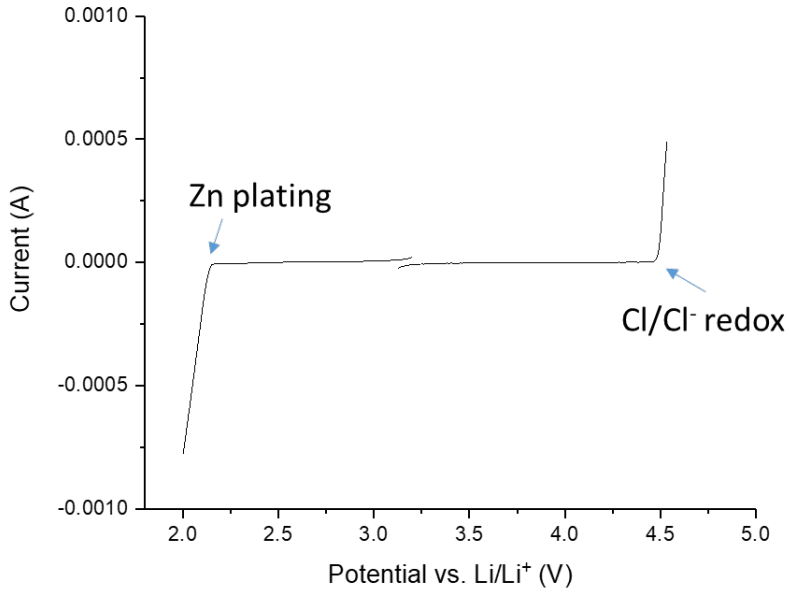

Figure 3.9 CV measurement of glassy carbon /$Li_2ZnCl_4.9H_2O$/activated carbon cell in the voltage range between 2.2 V to 4.5V vs. Li/Li^+ at the scanning rate of 5 $mV.s^{-1}$.

Chapter 4: Electrochemical Performance at extreme temperatures

4.1 Electrochemical Performance at room temperature

All the electrochemical cells utilize $Li_2ZnCl_4.xH_2O$ (x=6,9,12) as electrolytes and a cathode composite comprised of 10 wt. % PTFE as binder and 10 wt. % Carbon Black and 80 wt. % u-LFP or c-LFP as active material and the zinc foil as anode. Figure 4.1 shows cycling performance of the assembled cells containing c-LFP1,c-LFP2, c-LFP3 or u-LFP during the fifty charge/discharge cycles at a constant current rate of 0.3C for $LiFePO_4$ at the room temperature. All the three samples demonstrated a stable cycle performance, which is one of the distinct properties of the $LiFePO_4$. The u-LFP maintains a specific capacity of round 130 $mAh.g^{-1}$. The specific capacity values are increasing in the sequence of decreasing PEDOT coating. For the c-LFP1, the $LiFePO_4$ coated with the most amount of PEDOT, the specific capacity is much lower than that of the pristine $LiFePO_4$, which indicated that c-LFP1 loses near 25% of original capacity due to excessive coating of PEDOT. For the c-LFP2 and c-LFP3, their capacities maintain roughly same values as that of pristine $LiFePO_4$. Especially for the c-LFP3, the specific capacity is a little bit higher than that of pristine $LiFePO_4$. The cycle performances of three cells with PEDOT-coated $LiFePO_4$ still show the evident properties of pristine $LifePO_4$. Besides, the existence of PEDOT decreases the overpotential as shown in Fig 4.2. The overpotential is minimal with 57.3 mV in the c-LFP2 (8.3 wt.% PEDOT), indicating enhancement of electronic

conductivity and lithium ion diffusion of cathode material which are main issues at low temperature.

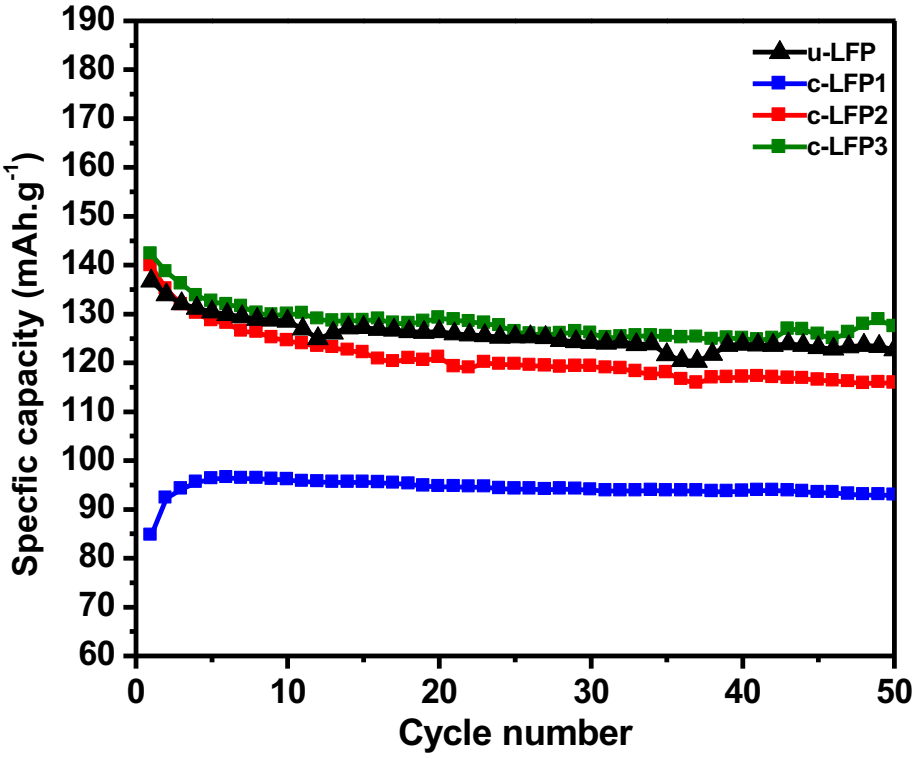

Fig 4.1 Cycling performance of PEDOT-coated $LIFePO_4$ electrodes, c-LFP1 (blue), c-LFP2 (red) and c-LFP3 (green) comparing with uncoated $LiFePO_4$, u-LFP (black) (current density= 0.3C, temperature=25 ℃)

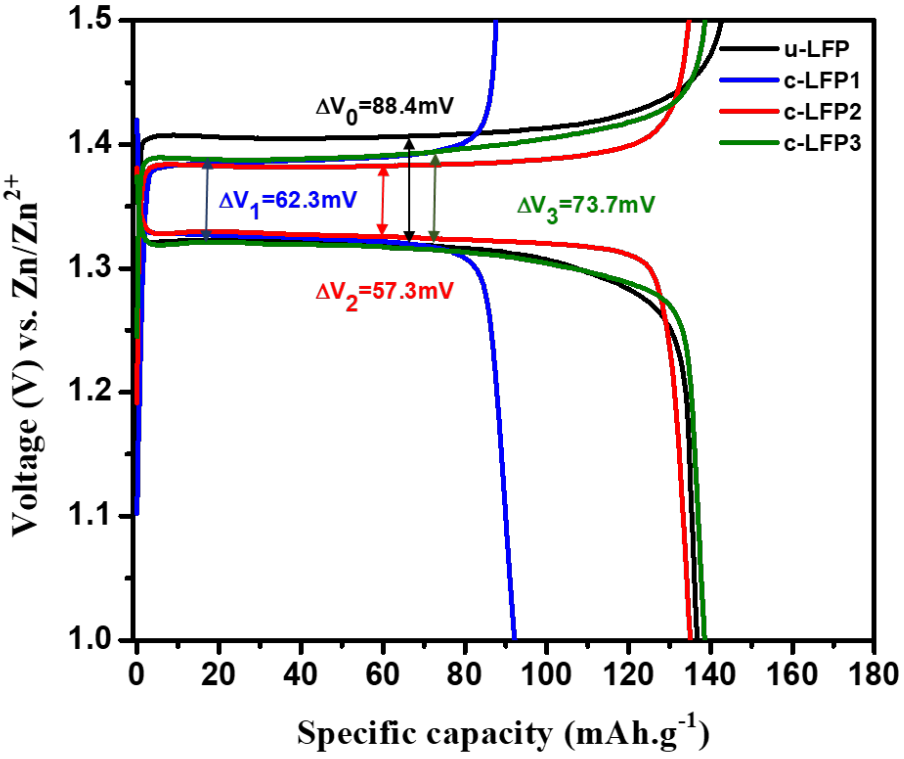

Fig 4.2 Charge-discharge curves of PEDOT-coated $LIFePO_4$ electrodes at first cycle, c-LFP1 (red), c-LFP2 (blue) and c-LFP3 (green) comparing with uncoated $LiFePO_4$, u-LFP (black) (current density= 0.3C, temperature=25 ℃)

4.2 Electrochemical Performance at 70 ℃

For the electrochemical test at 70℃, the assembled zinc batteries containing the electrodes comprising c-LFP1, c-LFP2, c-LFP3 or u-LFP and three concentrations of electrolytes of Li_2ZnCl_4 are compared in Fig 4.3. At the elevated temperature, the c-$LiFePO_4$/Zn cells shows a slight higher capacity than those containing same electrolytes and cathodes at room temperature, mainly because the resistance of cell

and ion mobility in the electrolyte and the electrode wetting are improved at 70℃.

For the electrolytes, the columbic efficiency increases with increasing concentration of Li_2ZnCl_4. Especially for the cell with c-LFP3 in the electrolyte $Li_2ZnCl_4.6H_2O$, the CE is ~99.5% at first twenty cycles and the capacity degrades from 140.5 $mAh.g^{-1}$ to 114 $mAh.g^{-1}$. However, the best combination of coating and electrolyte is the cell with c-LFP2 in the electrolyte $Li_2ZnCl_4.9H_2O$, which has highest specific capacity of 156 $mAh.g^{-1}$ and degraded to 130 $mAh.g^{-1}$ after 20 cycles with 94~99% CE during first twenty cycles. After the charge/discharge test in the high temperature, the c-LFP2 with the electrolyte $Li_2ZnCl_4.9H_2O$ is considered as having best electrochemical performance.

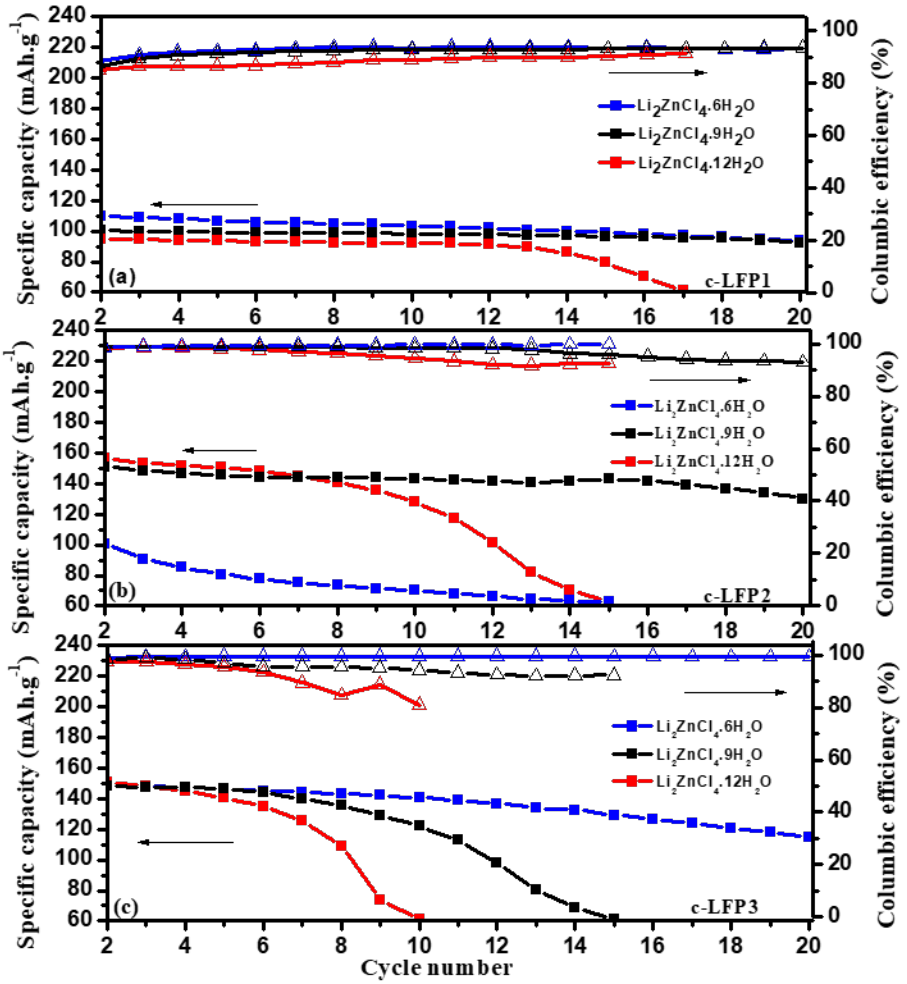

Figure 4.3 Cycling performance of $Li_2ZnCl_4.6H_2O$ (blue), $Li_2ZnCl_4.9H_2O$ (black), $Li_2ZnCl_4.9H_2O$ (red) with different electrodes c-LFP1 (a), c-LFP2 (b) and c-LFP3 (c), respectively during 20 cycles (current density= 0.3C, temperature=70 ℃)

Figure 4.4 compares the discharging potential curves for the cell containing c-LFP2 and the cell containing u-LFP in the same electrolyte $Li_2ZnCl_4.9H_2O$ at first twenty cycles under the rate of 0.3C at 70℃. The electrochemical performance of PEDOT-coated $LiFePO_4$ materials showed higher specific capacity and better capacity retention compared to the uncoated $LiFePO_4$ at elevated temperature. In the

first cycle, the specific capacity of c-LFP2 is 156 $mAh.g^{-1}$, higher than 127 $mAh.g^{-1}$ of u-LFP. During the 10^{th} cycle, the capacity of u-LFP retains 82.7% of first cycle discharging capacity, while the capacity of c-LFP-2 retains 91.7% of first cycle discharging capacity. The improved capacity retention of c-LFP2 at 20^{th} cycle is more evident. Compared with 52.0% capacity retention of u-LFP during first twenty cycles, the capacity of c-LFP2 faded to 130 $mAh.g^{-1}$ with the retention of 83.4%. To sum up, the positive effect of the PEDOT and $Li_2ZnCl_4.9H_2O$ in reducing capacity fading and increasing specific capacity of the type of cell $LiFePO_4$/Zn is distinct at elevated temperature, which are attributed to improving the poor electrical contact of $LiFePO_4$ and high ionic conductivity of electrolyte, respectively. Simultaneously, the coating and the $Li_2ZnCl_4.9H_2O$ keep the fundamental nature of the lithiation/de-lithiation chemistry of $LiFePO_4$ at elevated temperature as that at room temperature.

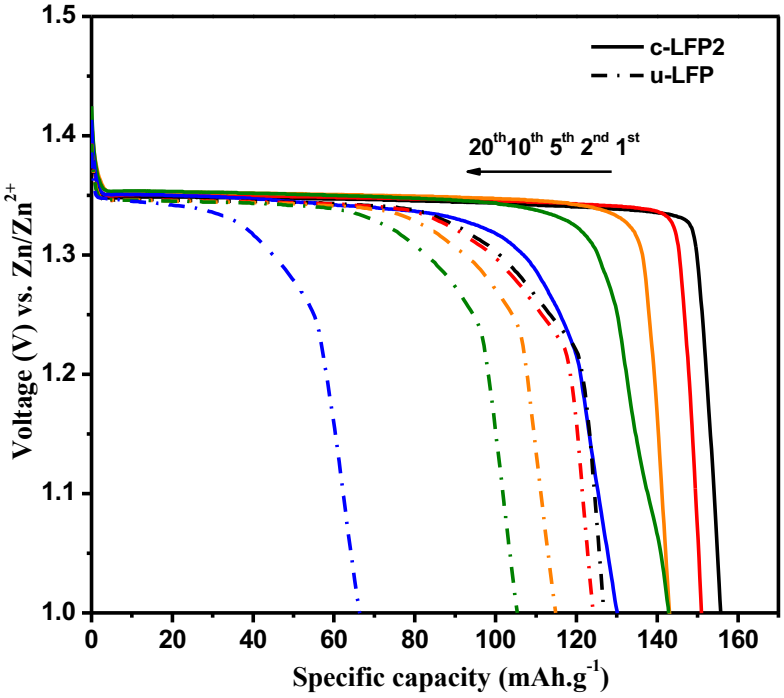

Figure 4.4 Discharge curves of c-LFP2 (solid line) electrode comparing with u-LFP (dash line) in $Li_2ZnCl_4.9H_2O$ (current density = 0.3C, temperature= 70 ℃)

For the rate behavior, the cell with c-LFP2 cathode in the $Li_2ZnCl_4.9H_2O$ as showed in Fig 4.5, tested at 70℃ during 30 cycles with variable current rates. At an intermediate rate of 0.5C, close to 93% of the capacity at rate of 0.3C was accessible. At a very high 10C rate, ~67% of original capacity was accessible. When the current rate return to original cycling with 0.3 C rate at the 26th cycle, the capacity reached to 136.5 mAh.g^{-1}, lost ~1.7 % of the 5th cycle at the rate of 0.3C. Thus, it showed a good rate capability at the elevated temperature due to the effect of highly conductive PEDOT on increasing electrical conductivity and lithium diffusion of cathode.

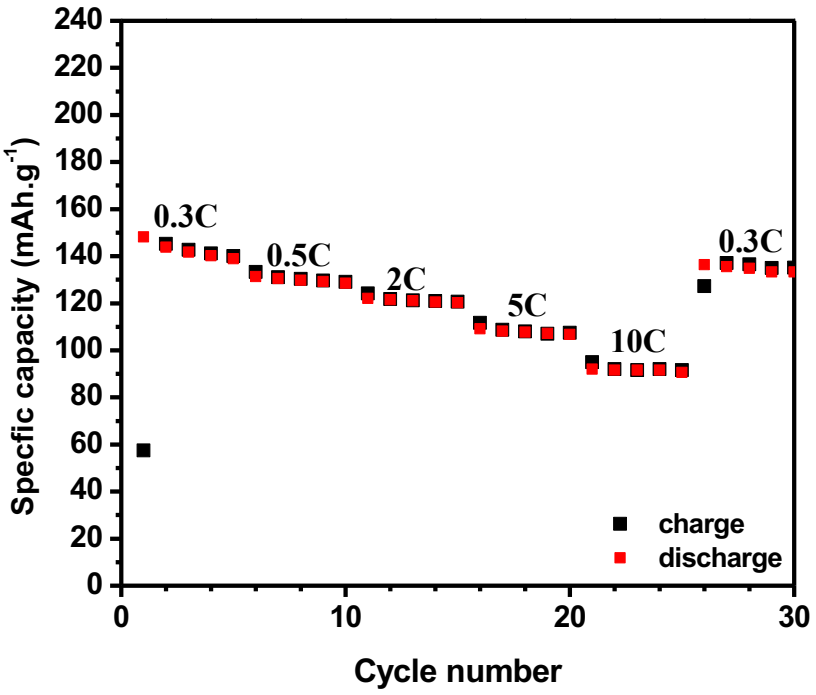

Figure 4.5 Rate capability of c-LFP2 electrode in $Li_2ZnCl_4.9H_2O$ at different current densities during 30 cycles (temperature=70 ℃)

4.3 Electrochemical Performance at -70 ℃

The electrolyte $Li_2ZnCl_4.6H_2O$ was also tried to operate at -70℃ because of a high columbic efficiency with ~99.5%. However, the electrolyte was frozen at extremely low temperature. Thus, for the electrochemical test at the low temperature, the cell was constructed by the c-LFP2 as cathode and $Li_2ZnCl_4.9H_2O$ as electrolyte due to the excellent electrochemical performance at elevated temperature. The cell was measured at the rate of 0.1C at -70℃ for 50 cycles in Fig 4.6. At the first six

cycles, the capacity increased from 101 $mAh.g^{-1}$ to 150.2 $mAh.g^{-1}$. The discharging curve shows a single plateau

at ~1.78 V vs. Zn/Zn^{2+}, which is distinct higher than the standard plateau of $LiFePO_4$ vs. Zn (1.18V at 25 ℃) At low temperature, there may exists a phase transition of $LiFePO_4$ or metal Zn leading the distinct difference of potential, which was not studied at this research. At the 6th cycle, the c-LFP2/Zn cell showed a maximum capacity of 150.2 $mAh.g^{-1}$ and the capacity faded gradually with continuous cycle, retaining 134.3 $mAh.g^{-1}$ with 89.45% of highest achievable capacity after 50 cycles. Fig 4.7 indicates an excellent cycling stability of the cell at extreme low temperature.

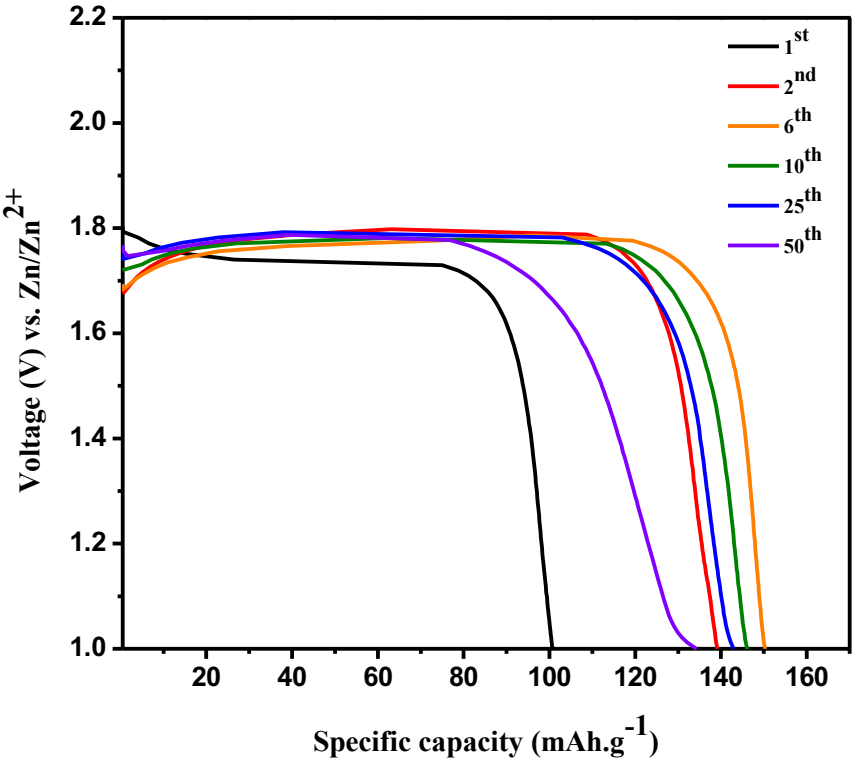

Figure 4.6 Discharge curves of c-LFP2 electrode in $Li_2ZnCl_4.9H_2O$ (current density=0.1C, temperature= -70 ℃)

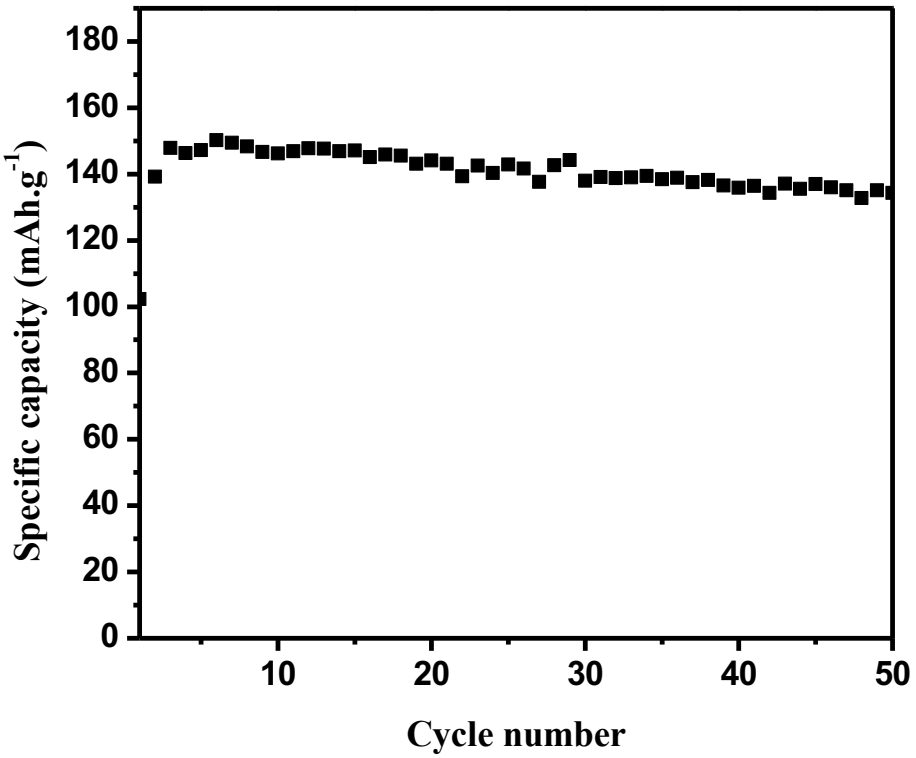

Figure 4.7 Cycling performance of c-LFP2 electrode in $Li_2ZnCl_4.9H_2O$ during 50 cycles (current density=0.1C, temperature= -70 ℃)

Chapter 5: Conclusion

In order to broadening the operating temperature limitation of battery, the aqueous PEDOT-coated $LiFePO_4$/ Zn battery using $Li_2ZnCl_4.9H_2O$ electrolyte was developed, which can be operated in the unprecedented operating temperature range from -70 ℃ to 70 ℃. We systematically investigated the concentration of superionic electrolyte $Li_2ZnCl_4.xH_2O$ to achieve maximum ionic conductivity in the temperature range between -70 ℃ and +70 ℃. The optimized $Li_2ZnCl_4.9H_2O$ (8.5 $mol.kg^{-1}$) has highest conductivity (σ=0.207 $S.cm^{-1}$ at 70℃, σ=1.002 $mS.cm^{-1}$ at -70℃) in the wide temperature range and can support the PEDOT-coated $LiFePO_4$/Zn battery to operate in the temperature from -70 ℃ and +70 ℃, especially for increasing the sluggish lithium ion transport at -70 ℃. Moreover, coating a layer of electronic conductive PEDOT on $LiFePO_4$ can significantly reduce the reaction of $LIFePO_4$ with electrolytes enhancing cycling stability, especially at elevated temperature. At 70 ℃, PEDOT-coated $LiFePO_4$/Zn using electrolyte $Li_2ZnCl_4.9H_2O$ shows high specific capacity of 156 $mAh.g^{-1}$ and the capacity still maintain at 130 $mAh.g^{-1}$ after 20 cycles at the rate of 0.3C. It also exhibited a good rate capability with capacities of 122 $mAh.g^{-1}$ at 2 C and 92 $mAh.g^{-1}$ at 10 C. Besides, the $LiFePO_4$/Zn also shows high performance at extreme low temperature of -70 ℃. It showed an excellent cycle stability with high reversible capacity. The high specific capacity of 149 $mAh.g^{-1}$ was achieved and 89.45% of highest capacity was retained after 50 cycles at the rate of 0.1C at -70℃.

Chapter 6: Future Work

1. Further investigation is needed in studying the reason why the discharging plateau of PEDOT-coated LiFePO4/Li2ZnCl4.9H2O/Zn of 1.78 V at low temperature is much higher than the standard potential of LiFePO4

2. Based on the electrochemical performance at elevated temperature, although the cathode PEDOT-coated LiFePO4 in Li2ZnCl4.9H2O decreased capacity degradation distinctly and increase cyclability comparing with pristine $LiFePO_4$, the modification of $LiFePO_4$ and electrolytes should be improved in order to increasing the cycle life at elevated temperature.

3. Although some characterization of $Li_2ZnCl_4.xH_2O$ have been investigated, limited studies of the mechanism of electrolyte $Li_2ZnCl_4.xH_2O$ system for high performance at extreme temperatures. More about the cation-solvent interaction needs to be studied.

Bibliography

1. Poizot, P.; Dolhem, F., Clean energy new deal for a sustainable world: from non-CO 2 generating energy sources to greener electrochemical storage devices. *Energy & Environmental Science* 2011, 4, 2003-2019.
2. Manthiram, A., Materials challenges and opportunities of lithium ion batteries. *The Journal of Physical Chemistry Letters* 2011, 2, 176-184.
3. Suo, L.; Borodin, O.; Gao, T.; Olguin, M.; Ho, J.; Fan, X.; Luo, C.; Wang, C.; Xu, K., "Water-in-salt" electrolyte enables high-voltage aqueous lithium-ion chemistries. *Science* 2015, 350, 938-943.
4. Alias, N.; Mohamad, A. A., Advances of aqueous rechargeable lithium-ion battery: A review. *Journal of Power Sources* 2015, 274, 237-251.
5. Zhang, J.; Zhang, L.; Liu, H.; Sun, A.; Liu, R.-S., *Electrochemical technologies for energy storage and conversion*. John Wiley & Sons: 2012.
6. Beck, F.; Rüetschi, P., Rechargeable batteries with aqueous electrolytes. *Electrochimica Acta* 2000, 45, 2467-2482.
7. Li, W.; Dahn, J. R., Lithium‐Ion Cells with Aqueous Electrolytes. *Journal of the Electrochemical Society* 1995, 142, 1742-1746.
8. Yang, C.; Chen, J.; Qing, T.; Fan, X.; Sun, W.; von Cresce, A.; Ding, M. S.; Borodin, O.; Vatamanu, J.; Schroeder, M. A., 4.0 V Aqueous Li-Ion Batteries. *Joule* 2017, 1, 122-132.
9. Mi, C.; Zhang, X.; Li, H., Electrochemical behaviors of solid LiFePO4 and Li0. 99Nb0. 01FePO4 in Li2SO4 aqueous electrolyte. *Journal of Electroanalytical Chemistry* 2007, 602, 245-254.
10. Nakayama, N.; Nozawa, T.; Iriyama, Y.; Abe, T.; Ogumi, Z.; Kikuchi, K., Interfacial lithium-ion transfer at the LiMn2O4 thin film electrode/aqueous solution interface. *Journal of Power Sources* 2007, 174, 695-700.
11. Ruffo, R.; La Mantia, F.; Wessells, C.; Huggins, R. A.; Cui, Y., Electrochemical characterization of LiCoO2 as rechargeable electrode in aqueous LiNO3 electrolyte. *Solid State Ionics* 2011, 192, 289-292.
12. Zhao, M.; Zhang, B.; Huang, G.; Zhang, H.; Song, X., Excellent rate capabilities of (LiFePO4/C)//LiV3O8 in an optimized aqueous solution electrolyte. *Journal of Power Sources* 2013, 232, 181-186.
13. Porcher, W.; Moreau, P.; Lestriez, B.; Jouanneau, S.; Le Cras, F.; Guyomard, D., Stability of LiFePO 4 in water and consequence on the Li battery behaviour. *Ionics* 2008, 14, 583-587.
14. Hull, S., Superionics: crystal structures and conduction processes. *Reports on Progress in Physics* 2004, 67, 1233.
15. Nagel, R.; Groß, T. W.; Günther, H.; Lutz, H., 6Li and 7Li MAS NMR Studies on Fast Ionic Conducting Spinel-Type Li2MgCl4, Li2–xCuxMgCl4, Li2–xNaxMgCl4, and Li2ZnCl4. *Journal of Solid State Chemistry* 2002, 165, 303-311.
16. Kanno, R.; Takeda, Y.; Yamamoto, O.; Cros, C.; Gang, W.; Hagenmuller, P., Ionic Conductivity and Phase Transition of the Bromide Spinels, Li2− 2x M 1+ x Br4 (M= Mg, Mn). *Journal of The Electrochemical Society* 1986, 133, 1052-1056.

17. Kanno, R.; Takeda, Y.; Mori, M.; Yamamoto, O., Ionic Conductivity and Structure of Double Chloride Li2ZnCl4 in the LiCl–ZnCl2 System. *Chemistry Letters* 1989, 18, 223-226.
18. Xu, C.; Li, B.; Du, H.; Kang, F., Energetic zinc ion chemistry: the rechargeable zinc ion battery. *Angewandte Chemie International Edition* 2012, 51, 933-935.
19. Trócoli, R.; La Mantia, F., An Aqueous Zinc‐Ion Battery Based on Copper Hexacyanoferrate. *ChemSusChem* 2015, 8, 481-485.
20. Wang, F.; Borodin, O.; Gao, T.; Fan, X.; Sun, W.; Han, F.; Faraone, A.; Dura, J. A.; Xu, K.; Wang, C., Highly reversible zinc metal anode for aqueous batteries. *Nature Materials* 2018, 1.
21. Zhang, B.; Liu, Y.; Wu, X.; Yang, Y.; Chang, Z.; Wen, Z.; Wu, Y., An aqueous rechargeable battery based on zinc anode and Na 0.95 MnO 2. *Chemical Communications* 2014, 50, 1209-1211.
22. Zhang, H.; Du, Q.; Li, C.; Sun, X., Binary Ion Batteries Operating on the Model of Newton's Cradle. *Journal of The Electrochemical Society* 2012, 159, A2001-A2004.
23. Idota, Y.; Kubota, T.; Matsufuji, A.; Maekawa, Y.; Miyasaka, T., Tin-based amorphous oxide: a high-capacity lithium-ion-storage material. *Science* 1997, 276, 1395-1397.
24. Zhang, H.; Wu, X.; Yang, T.; Liang, S.; Yang, X., Cooperation behavior between heterogeneous cations in hybrid batteries. *Chemical Communications* 2013, 49, 9977-9979.
25. Rodrigues, M.-T. F.; Babu, G.; Gullapalli, H.; Kalaga, K.; Sayed, F. N.; Kato, K.; Joyner, J.; Ajayan, P. M., A materials perspective on Li-ion batteries at extreme temperatures. *Nature Energy* 2017, 2, 17108.
26. Mandal, B. K.; Padhi, A. K.; Shi, Z.; Chakraborty, S.; Filler, R., New low temperature electrolytes with thermal runaway inhibition for lithium-ion rechargeable batteries. *Journal of power sources* 2006, 162, 690-695.
27. Chen, K.; Yu, Z.; Deng, S.; Wu, Q.; Zou, J.; Zeng, X., Evaluation of the low temperature performance of lithium manganese oxide/lithium titanate lithium-ion batteries for start/stop applications. *Journal of Power Sources* 2015, 278, 411-419.
28. Amine, K.; Liu, J.; Belharouak, I., High-temperature storage and cycling of C-LiFePO4/graphite Li-ion cells. *Electrochemistry communications* 2005, 7, 669-673.
29. Chang, H.-H.; Chang, C.-C.; Su, C.-Y.; Wu, H.-C.; Yang, M.-H.; Wu, N.-L., Effects of TiO2 coating on high-temperature cycle performance of LiFePO4-based lithium-ion batteries. *Journal of Power Sources* 2008, 185, 466-472.
30. Zhang, H.; Xu, Y.; Zhao, C.; Yang, X.; Jiang, Q., Effects of carbon coating and metal ions doping on low temperature electrochemical properties of LiFePO4 cathode material. *Electrochimica Acta* 2012, 83, 341-347.
31. Yang, J.; Kim, D. H.; Hendricks, J. L.; Leach, M.; Northey, R.; Martin, D. C., Ordered surfactant-templated poly(3,4-ethylenedioxythiophene) (PEDOT) conducting polymer on microfabricated neural probes. *Acta Biomaterialia* 2005, 1, 125-136.
32. Liu, X.; Li, H.; Ishida, M.; Zhou, H., PEDOT modified LiNi1/3Co1/3Mn1/3O2 with enhanced electrochemical performance for lithium ion batteries. *Journal of power sources* 2013, 243, 374-380.

33. Ma, D.-l.; Cao, Z.-y.; Wang, H.-g.; Huang, X.-l.; Wang, L.-m.; Zhang, X.-b., Three-dimensionally ordered macroporous FeF 3 and its in situ homogenous polymerization coating for high energy and power density lithium ion batteries. *Energy & Environmental Science* 2012, 5, 8538-8542.
34. Yao, Y.; Liu, N.; McDowell, M. T.; Pasta, M.; Cui, Y., Improving the cycling stability of silicon nanowire anodes with conducting polymer coatings. *Energy & Environmental Science* 2012, 5, 7927-7930.
35. Dinh, H.-C.; Yeo, I.-H.; Cho, W. I.; Mho, S.-i., Characteristics of conducting polymer-coated nanosized LiFePO4 cathode in the Li+ batteries. *ECS Transactions* 2010, 28, 167-175.
36. Damlin, P.; Kvarnström, C.; Ivaska, A., Electrochemical synthesis and in situ spectroelectrochemical characterization of poly (3, 4-ethylenedioxythiophene)(PEDOT) in room temperature ionic liquids. *Journal of Electroanalytical Chemistry* 2004, 570, 113-122.
37. Zhan, L.; Song, Z.; Zhang, J.; Tang, J.; Zhan, H.; Zhou, Y.; Zhan, C., PEDOT: Cathode active material with high specific capacity in novel electrolyte system. *Electrochimica Acta* 2008, 53, 8319-8323.
38. Corradi, R.; Armes, S., Chemical synthesis of poly (3, 4-ethylenedioxythiophene). *Synthetic metals* 1997, 84, 453-454.
39. Zhang, Y.; Sun, H.; Cao, J.; Chen, S.; Dong, L.; Xing, H.; Duan, X.; Xu, J., Preparation and characterization of poly (2′-aminomethyl-3, 4-ethylenedioxythiophene) by chemical oxidative polymerization. *Polymer Science, Series B* 2017, 59, 586-590.
40. University of Cambridge, Linear Sweep and Cyclic Voltametry: The Principles. *https://www.ceb.cam.ac.uk/research/groups/rg-eme/teaching-notes/linear-sweep-and-cyclic-voltametry-the-principles* 2015.
41. Yamaguchi, T.; Hayashi, S.; Ohtaki, H., X-ray diffraction and Raman studies of zinc (II) chloride hydrate melts, ZnCl2. rH2O (r= 1.8, 2.5, 3.0, 4.0, and 6.2). *The Journal of Physical Chemistry* 1989, 93, 2620-2625.
42. Moyer, J.; Evans, J.; Lo, G. S., A Raman Spectroscopic Study of the Molten Salt System ZnCl2-KCl. *Journal of The Electrochemical Society* 1966, 113, 158-161.
43. Kanno, H.; Hiraishi, J., Raman spectroscopic study of glassy aqueous zinc halide solutions. *Journal of Raman Spectroscopy* 1980, 9, 85-89.